A NEW ANALYTCAL MODEL FOR

TOOL LIFE

IN

METAL STAMPING

A NEW ANALYTICAL MODEL FOR TOOL LIFE IN METAL STAMPING

By

ABDUL VALI SYED, B.E, M.Tech.

A Thesis

Submitted to the School of Graduate Studies

In Partial Fulfillment of the Requirements

for the Degree

Master of Applied Science

McMaster University

MASTER OF APPLIED SCIENCE (2006) McMaster University

(Mechanical Engineering) Hamilton, Ontario

TITLE: A New Analytical Model for Tool Life in Metal Stamping

AUTHOR: Abdul V.Syed, B.E. (Mech. Engineering), Osmania University, India.

M.Tech. (Production Engineering), TRTC, Delhi, India.

SUPERVISOR: Dr. Mukesh K. Jain

Department of Mechanical Engineering

McMaster University

NUMBER OF PAGES: xix, 130

Abstract

Tool life during the precision stamping of stainless steel sheet (AISI 301) has been studied with particular emphasis on reduction in the punch diameter and part hole size due to tool wear. Two analytical models for predicting tool life in terms of number of quality parts that could be stamped between two re-grindings have been proposed using a combination of Archard's wear model and punching force. The proposed tool life models have been verified by experiment trials with a round M2 punch and die. The trials were carried out on a precision progressive die in an industrial environment.

The first tool life model calculates the pierced hole diameter variation for a given tool from sheet material properties and gives an estimation of number of parts that could be stamped for a given tolerance on a hole size. The second tool life model calculates number of parts with respect to the allowed burr height. Both of the proposed models are derived using sheet material properties such as sheet thickness, strength coefficient (K), strain hardening index (n) and material elongation (A); process parameters such as die clearance and friction coefficient; punch characteristics such as normalized wear rate, punch diameter and punch edge radius. Finite element analysis was also employed to simulate the hole piercing process to predict burr height. The results from the proposed tool life models, FE modeling and the experiments are in good agreement.

Acknowledgements

I would like to express my sincere gratitude to my supervisor, Dr. Mukesh K. Jain, for giving me a chance to complete this innovative research, his constructive guidance and support throughout this project.

I would also like to heartfully thank Dr. German Fox-Rabinovich for his valuable assistance in understanding material science involved in metal stamping. I would also like to sincerely thank Dr. Michael Bruhis for his valuable assistance in conducting this research and Mr. Quan Situ for advice on finite element analysis.

I would also like to acknowledge my industrial supervisors Mr. Andrew Jones and Mr. Mulak Gulati for valuable assistance in conducting this research at OPPLAST. I would like to thank Mr. Heiner Ophard, President and Mr. Tony Snider, Vice Prseident of OPPLAST for giving me an opportunity and support for completing my research at OPPLAST works. Support of my friends and colleagues is also acknowledged.

Finally, I would like to specially thank my parents, my wife and daughter and other family members for their encouragement and support.

Contents

List of Figures

List of Tables

Nomenclature

a_N	Minimum length of the side of the punch	Equation (3-6)
a	Maximum length of the side of the punch	Equation (3-6)
A	Initial punch area	Equation (3-2)
A_N	Punch area after N number of punching	Equation (3-2)
A_S	Shear area	Equation (2-2)
b	Burr height	Equation (3-19)
c	Punch and die clearance	Figure (2-10)
C	Material elongation factor	Equation (3-20)
C_1	Material constant in Atkins model	Equation (2-4)
C_1	Work hardening factor in Klingenberg et al.	Equation (2-15)
C_2	Strength coefficient	Equation (2-15)
d	Punch displacement	Equation (2-3)
d_{peak}	Peak punch displacement	Equation (2-6)
D_N	Punch diameter after N number of punching	Equation (2-2)
D_P	Initial punch diameter	Equation (2-2)
f	Friction factor in Klingenberg et al.	Equation (2-3)
$f(x)$	Burr height at the beginning of punching	Equation (3-19)
$f(y)$	Burr height due to punch edge wear	Equation (3-19)
F	Normal force applied	Equation (2-20)
F	Shear force	Equation (2-2)
F_{blank}	Blanking force	Equation (2-13)

F_{shear}	Shear force	Equation (2-12)
h_0	Sheet thickness	Equation (2-2)
H	Punch hardness	Equation (2-20)
H_1	Depth of sheared edge	Equation (2-25)
H_C	Hardness of dispersed carbide	Equation (2-21)
H_m	Matrix hardness	Equation (2-21)
H_{ve}	Punch effective hardness	Equation (2-21)
I_m	Correction factor in Zhou et al. model	Equation (2-7)
k	Wear coefficient	Equation (2-20)
K	Strength coefficient	Equation (2-7)
K'	Normalized abrasive wear rate	Equation (2-22)
K''	Normalized adhesive wear rate	Equation (3-21)
$K(d)$	Bending factor in Klingenberg et al. model	Equation (2-13)(b)
K_{us}	Wear coefficient in Hambli model	Equation (2-23)
L	Length of cut	Equation (3-7)
M	Nodal mass matrix	Equation (5-1)
m	Initial punch weight	Equation (3-10)
m_N	Punch weight after N number of punching	Equation (3-10)
n	Strain hardening index in power law	Equation (2-1)
N	Number of punching strokes	Equation (3-2)
P	Nodal force	Equation (5-1)
Q	Shear force in Zhou et al. model	Equation (2-7)
R	Initial punch edge radius	Equation (3-20(a)

R_N	Punch edge radius after N number of punching	Equation (3-20)(b)
R_P	Punch radius	Equation (2-24)
R_{wd}	Die edge radius	Fig (2-10)
R_{wp}	Punch edge radius	Equation (2-24)
s	Sliding distance	Equation (2-20)
S	Punch travel	Equation (3-16)
S_f	Proportional factor in Ramaekers model	Equation (2-1)
t	Sheet thickness	Equation (2-25)
T	Total time of deformation	Equation (2-23)
u	Punch displacement	Equation (2-25)
$\ddot{u}$	Nodal accelerations	Equation (5-1)
V	Punch wear volume	Equation (2-20)
V_b	Punch/die wear volume in bending	Equation (7-1)
V_N	Punch wear volume after N number of punching	Equation (3-21)
w	Wear rate	Equation (2-20)
α	Angle of bend in Klingenberg et al. model	Equation (2-11)
τ	Shear strength	Equation (2-2)
σ_{uts}	Ultimate tensile strength	Equation (2-2)
ω	Punch die clearance	Figure (2-2)
γ	Shear strain	Equation (2-4)
γ_{peak}	Peak shear strain	Equation (2-6)
ς	Punch displacement function	Equation (2-7)
$\varphi(d)$	Bending factor in Zhou et al. model	Equation (2-12)

$\bar{\sigma}$	VonMises equivalent stress	Equation (2-16)
σ^e	Engineering stress	Equation (A-4)
σ^T	True stress	Equation (A-4)
σ_n	Normal stress acting on tool surface	Equation (2-23)
ε^e	Engineering strain	Equation (A-1)
$\bar{\varepsilon}$	VonMises equivalent strain	Equation (2-16)
ε^T	True strain	Equation (A-4)
ε^{pl}	Plastic strain	Equation (A-5)
ε^{el}	Elastic strain	Equation (A-5)
Δv	Sliding velocity between tool and workpiece	Equation (2-23)
δw	Wear depth	Equation (2-23)

Chapter 1

Introduction and Objectives

Metal stamping is a cost-effective process, because it is able to produce material-intensive parts at production rates that are much greater than what is possible using other traditional methods. Many parts that are being designed to undergo other metal fabrication processes, such as casting, die casting, forging or machining, could just as easily be designed for stamping. The quality, accuracy, function, wear life and appearance of parts can be greatly improved by suitably designing them for stamping. Metal stamping allows parts to be made of tougher and harder material than other processes allow. Also, deformation (work hardening) results in superior mechanical properties of the part. Metal stamping dies in many instances cost less than other tooling.

In general, stampings can be classified as precision and non-precision. Precision stampings are used in watches, clocks, instruments, electronics, computer hardware, aerospace, medical devices, etc., where the part has critical engineering fits and tolerances and plays a role in assembly and functioning of a particular product. Figure 1-1 shows a precision watch mechanism assembly and the sheet metal parts. Non-precision stampings are used in general hardware,

furniture, appliances, household, automotive, etc., where the part has general tolerances but is not considered to be critical.

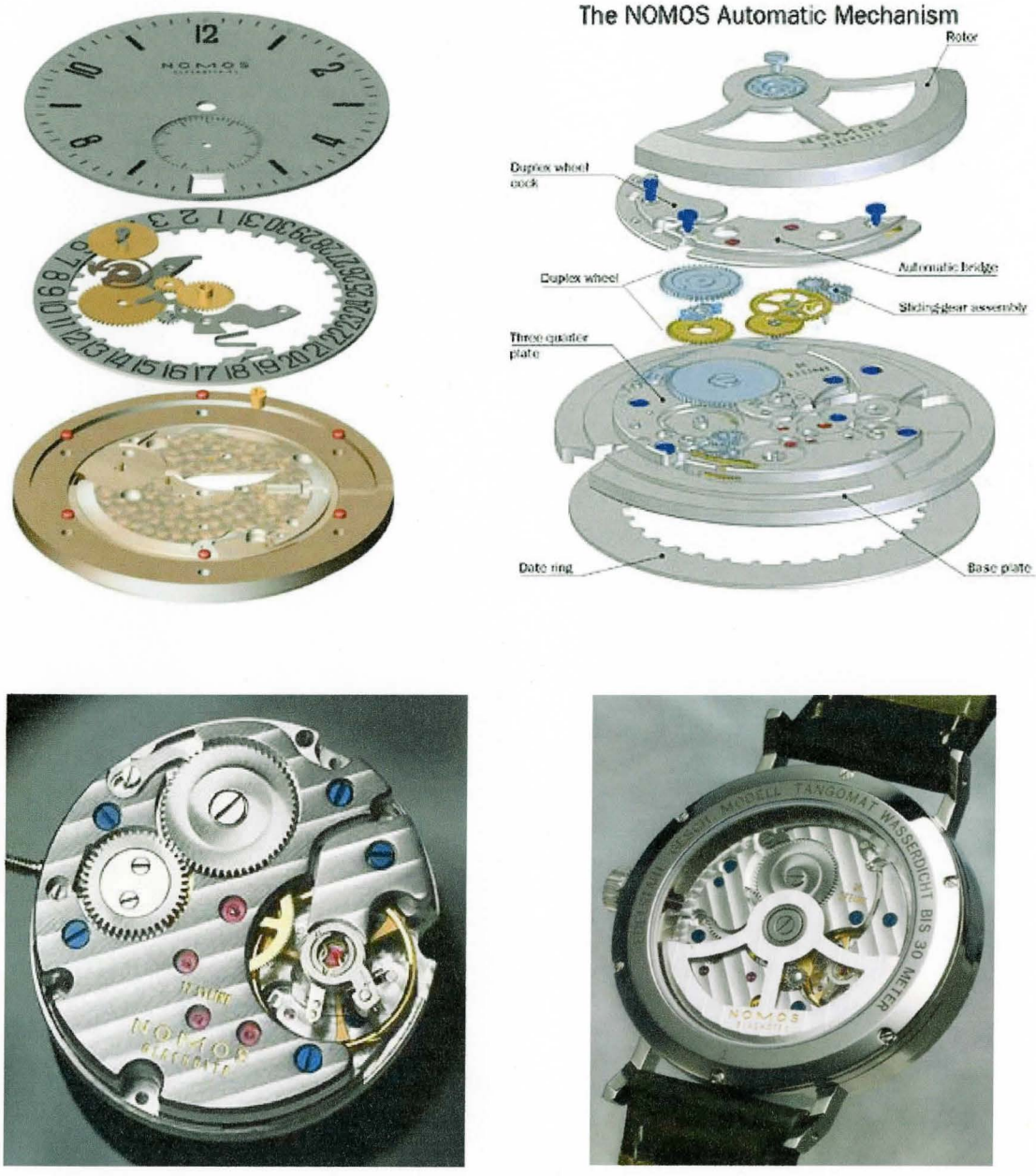

Figure 1-1 Watch mechanism having precision stamped metal parts [http://www.jardin-d-eden.co.uk/acatalog/Nomos_Watches.html].

1.1 Metal Stamping

1.1.1 Process

Metal stamping is a metal forming process in which flat stock sheet metal, formed from metals such as steel, brass, copper, aluminum, zinc, nickel, titanium, etc., is shaped into predetermined parts in a stamping press.

During press operation, the slide, or ram, maintains movement to and from a motionless table called a press bed (Figure 1-2). The die, a press tool consisting of a specially designed cavity, shapes metal parts from the inserted sheet metal. The upper component of the die connects to the press slide, and the lower component connects to the press bed. A die component called the punch performs the necessary shaping operation by pushing the sheet metal through the die.

The dies are several types such as single station blanking, trimming or compound dies; progressive or transfer dies; bending or forming dies. After the parts are formed, they are typically subjected to one or more secondary processes like deburring, heat treating and plating. Often the secondary processes can be reduced in number or eliminated altogether to reduce cost even further.

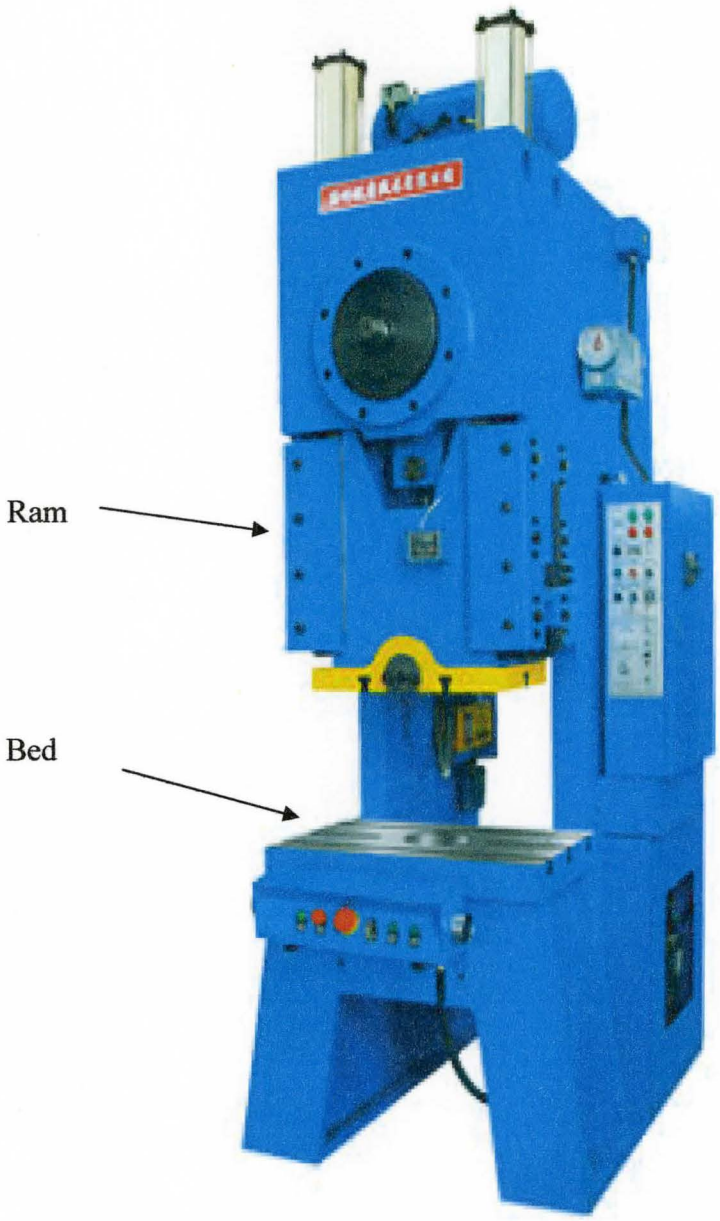

Figure 1-2 Stamping press [http://www.ugs.com/products/nx/docs/fs_mach_series_press.pdf].

1.1.2 Principles of Progressive Dies

A progressive die is used to transform a flat strip of metal into a completed part. This transformation is performed incrementally, or progressively, by a series of stations that cut, form and coin the material into the desired shape (Figure 1-3). The components that perform operations on the material are unique for every part. These components are located and guided in precision cut openings in plates which are in turn located and guided by pins.

A typical die cross section is shown in Figure 1-3 (c) and (d). The entire die is actuated by a mechanical press that moves the die up and down. The press is also responsible for feeding the material through the die, progressing it from one station to the next with each stroke. A typical strip layout of a progressive die is shown in Figure 1-3 (b). The individual die stations/stages of a strip layout would consist of various metal forming operations to shape the coiled strip into a final product. Shearing and bending are the two common metal forming operations in a high volume production of metal stampings. There are various shearing operations and are generally classified as follows:

- Punching/Piercing - in which a hole is cut in the part and the resulted slug is separated.
- Blanking - in which the slug is the part to be further processed.

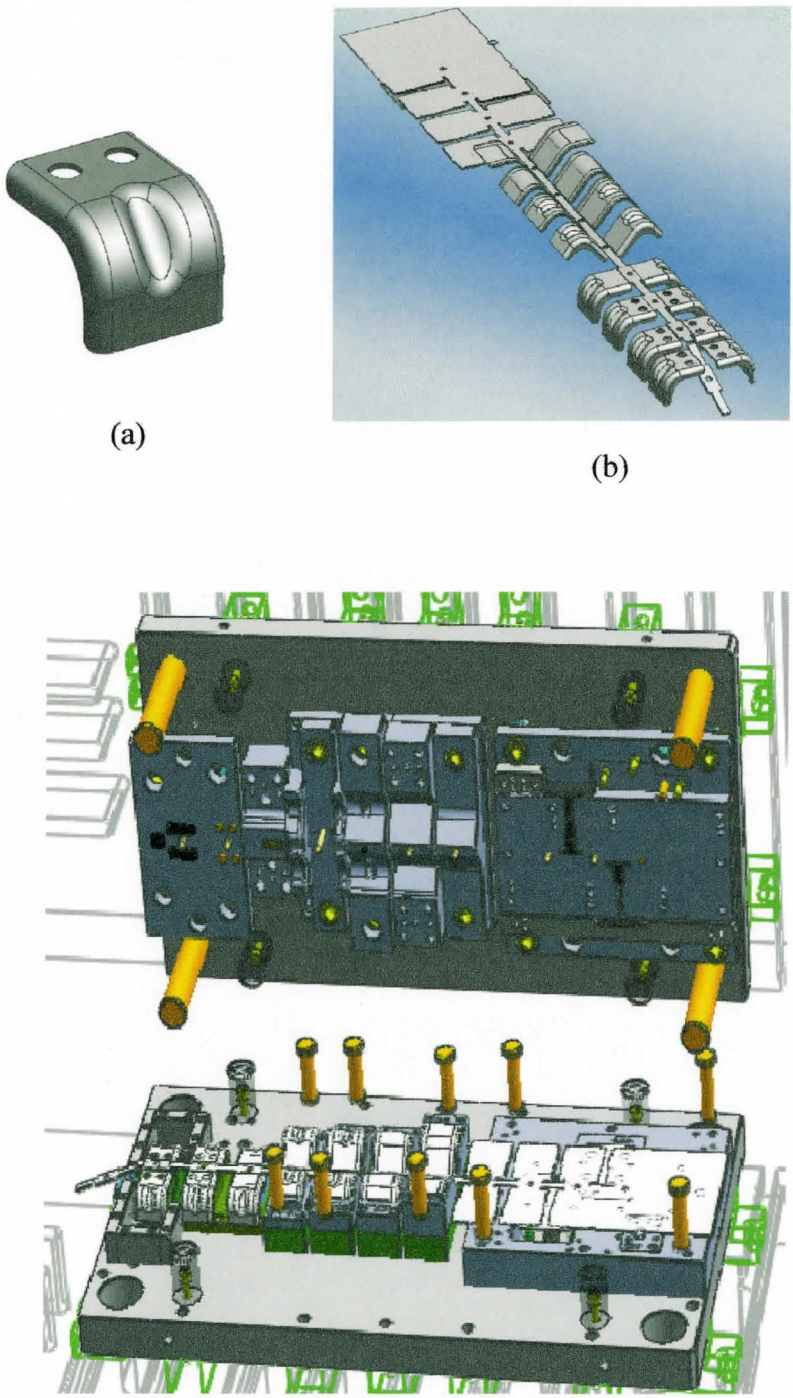

(a)

(b)

(c)

(d)

Figure 1-3 Elements of progressive die (a) part, (b) strip layout, (c) die -top half and (d) die- bottom half, [http://www.ugs.com/products/nx/docs/fs mach series progress.pdf].

1.2 Tool Life

The performance of the stamping dies is dependent on several factors, mainly: tool design, tool material, heat treatment of tool elements, tool manufacturing precision, work material, production conditions and tool maintenance. Any deviation in the quality of the above factors will have negative effects and results in tool failures. Tools have to be re-sharpened or replaced after they are failed to produce quality parts. Therefore, tool life in precision metal stamping is attributed by the number of parts stamped between two re-sharpenings.

1.2.1 Tool Failures

Important tool failure mechanisms include plastic deformation, chipping, galling and tool wear.

- Plastic deformation of the tool arises when the blanking force is high and the yield strength is locally exceeded. This problem could be eliminated either by increasing the hardness of the tool material while maintaining the toughness or by reducing the stress on the punch.

- Chipping is spontaneous and can not be planned for. Chipping may be due to inappropriate heat treatment, in-correct tool making or fatigue.

- Galling occurs when the work material is soft and adherent. Galling can be eliminated or minimized by reducing the friction by using a superior lubricant in the stamping process.

Therefore, plastic deformation, chipping and galling failures are often addressed first to improve the production process.

Tool wear is a process of slow degradation of punch surface caused by several mechanisms involved between punch and sheet material. Tool wear is the main topic of the present study and is discussed in detail in the following sections.

1.2.2 Tool Wear

Tool wear mechanisms include adhesive, abrasive, fatigue and diffusive wear. Adhesive and abrasive wear are the most common wear mechanisms that occur in blanking/piercing tooling when the surface of the working material contains hard particles, such as carbides or oxides. These

carbides or oxide particles are harder than the punches and will scratch the tool when the working material slides over the punch surfaces. Wear takes place on the external surface of the punch and causes punch edges to be rounded off (Figure 1-4).

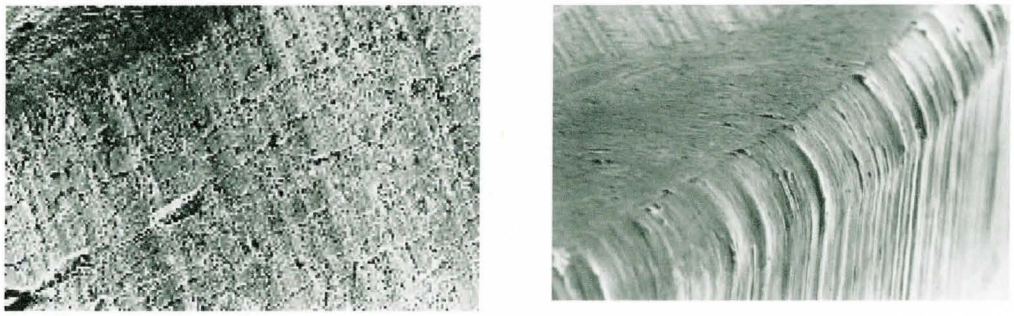

(a) (b)

Figure 1-4 SEM images of wear in stamping tools (a) adhesive wear and (b) abrasive wear [http://www.thefabricator.com/ToolandDie /ToolandDie_Article.cfm].

A review of punch wear is provided as follows [J. A. Schey, 1983]:

- The wear behavior at the punch surface considerably influences the quality of piercing/blanking. The tribological situation in piercing is typically characterized by high surface pressures, low deformation velocities and a variety of different friction conditions depending on the lubrication.

- The wear pattern is significantly affected by the properties of tool material, tool hardness, sheet material and clearance between punch and die.

- Elastic springback of the sheet material increases the pressure acting on the punch during retraction and thus increases flank wear, particularly in piercing a hole.

- Lateral or flank wear can be characterized by length or area. Flank wear is important because it determines the pierced hole size and punch length, which is lost in tool grinding. Its origin is in adhesion and abrasion and increases with number of punch strokes.

- Edge wear, even though it is difficult to separate from flank wear, is important in that it determines burr height. Edge wear also increases with number of punch strokes and is, at a minimum, at some fairly generous clearance (12%). Excessive clearance (17% or more) leads to a large burr, but only because the part is finally separated by tensile fracture, and not because of wear.

1.2.3 Tool Materials

The mechanism of tool wear and tool life in metal stamping is analyzed by various researchers and in turn different kinds of tool steels have been developed

to reduce the amount of wear. In addition to the development of new tool materials, various hard surface coatings are also developed to combat tool wear and improve tool life. Over the years, it is well understood that friction and wear can be predicted and minimized but can not be eliminated in metal stamping.

1.2.4. Tool Life in Metal Stampings

The main result of tool wear is the variation in part quality in terms of dimensions. The fits and tolerances in precision parts would be of the order of few micrometers and controls the accuracy of the instrument. Due to continuous punch wear, the size of the holes pierced by the worn punches becomes continuously under sized as the punching continues with the same punch. The punches and dies are re-sharpened after a certain amount of wear and until the quality of parts is acceptable.

Therefore, the tool life in metal stampings is expressed in terms of the number of parts stamped between two re-sharpenings and driven primarily by part dimensional tolerance. Prediction of tool life in terms of number of quality parts even before production would be a very useful tool in the present competitive environment.

1.3 Objective of Present Research

The present study is aimed at developing an analytical expression for tool life in metal stampings, in order to know the maximum number of stampings that can be produced between two re-sharpenings by defining:

- A model that quantifies punch wear and its influence on the size variation of a pierced hole.
- A model that estimates burr height due to punch edge wear.

A suitable tool life equation can help engineers and tool makers to:

- Plan tool maintenance schedules for regrinding and spare punches even before part production.
- Predict part dimensional variation in terms of number of strokes even before statistical process control (SPC).
- Determine the critical punches subjected to tool wear and help to select the right tool materials, clearances and process parameters.
- Compute the tool wear individually for every stage in a progressive die,
- Prepare accurate tooling quotes as this prediction helps to select right tool materials, number of regrindings for a given part tolerance.

A review of the past work on tool life in precision stamping dies is presented in Chapter 2. A new analytical model for tool life is developed in Chapter 3. Studies of hole piercing were carried out experimentally and corresponding methodology and results are described in Chapter 4.

FE modeling of hole piercing and simulation results with reference to the burr size is presented in Chapter 5. Tool life model predictions, FE simulations and comparisons with experimental results are reported in Chapter 6. A discussion of these results is presented in Chapter 7. Conclusions of present work and suggestions for future work are provided in Chapter 8. Supporting data used for ABAQUS/Explicit code is presented in the Appendix.

Chapter 2

Literature Review

2.1 Piercing/Blanking Process

Hole piercing/blanking operation is an important shearing process and is commonly used in progressive stamping dies. Since the beginning of year 1950, researchers have been analyzing the shearing process. Table 2-1 summarizes some of the previous research work relating process parameters and process outcomes on piercing/blanking.

Author and year	Tested parameters	Important results
Chang and Swift, 1950	Clearance, tool edge radius	Optimal clearance for ductile material
Johnson and Slater,1967	Clearance, punch speed, temperature	Load-displacement diagram
Johnson, 1973	Clearance	Effect of clearance on cut edge
Mielnik,1991	Clearance, load diagram	Reasons for load variation
Hambli, 2002	Clearance, tool wear, sheet thickness	Influence of material, tool, sources of error

Table 2-1 Previous research work on blanking/piercing.

The behavior of the pierced material during the shearing process can be divided into five stages which are illustrated with the typical force – displacement diagram [Johnson and Slater, 1967] as shown in the Figure 2-1.

During the start of the process, the sheet is pushed into the die and strip material is elastically deformed. The process continues and yield strength of the strip material is reached, first at the outer fibers and later at all the fibers in the zone between the punch and die. Normally the material underneath the punch is subject to thinning. Plastic deformation results in a rounding of the edge of the slug.

During this stage, or possibly as early as during the plastic deformation stage, damage initiation followed by the nucleation and growth of cracks takes place. In most of the conventional piercing/blanking situations, ductile fracture occurs after shear deformation. This causes rough, dimpled rupture morphology at the fractured surface of the product. Finally, the work done due to friction is dissipated when forcing (pushing) the slug through the die hole.

The quality and accuracy of piercing can be affected by clearance between punch and die, mechanical properties of the sheet metal, speed of the punch, thickness of the sheet and importantly the state of cutting edges and lubrication [J. A. Schey, 1983].

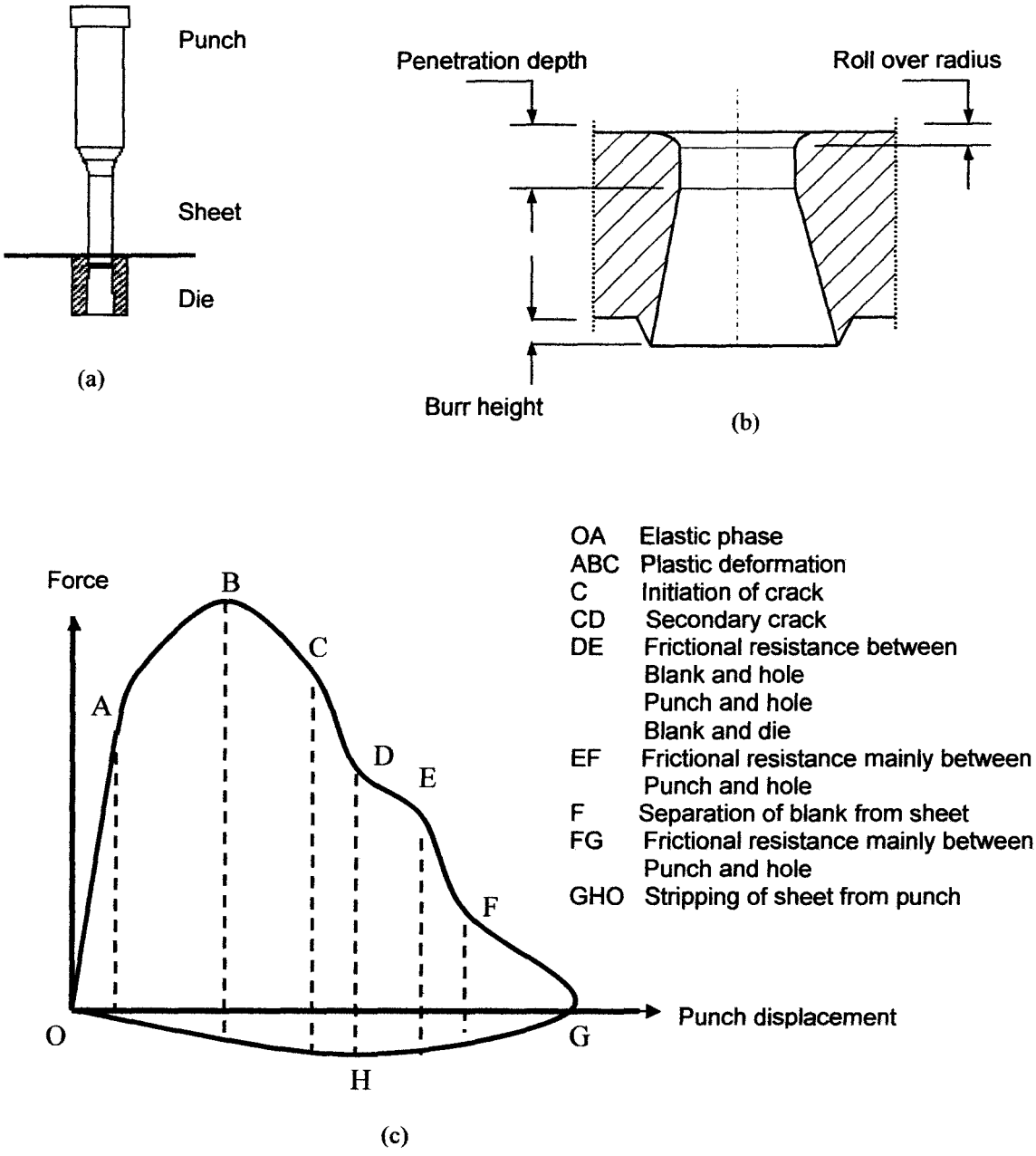

Figure 2-1 Example of hole piercing (a) elements of hole piercing, (b) typical characteristics of pierced hole and (c) force –displacement curve.

2.2 Analytical Models for Piercing/Blanking Process

Fundamental studies of blanking process have been carried out by many researchers, for example [Zunckler, 1963], [Kramer, 1969] and [Ramaekers, 1986].

Zunckler et. al assumed, based on inspection of the blank material that the plastic strains and distortions take place in a localized region in a lens shape. The shape was used as a boundary condition in which the flow of the material was described. However, the clearance between punch and die was not considered and the analysis did not produce any expression for the punch force.

Further studies were done by Atkins [Atkins, 1980] and Zhou and Wierzbicki [Zhou and Wierzbicki, 1996]. Atkins model was based on the assumption of pure shear, while Zhou et. al proposed a tension model. Recently, another model has been proposed by Klingenberg et. al [W. Klingenberg and U.P.Singh, 2004] while combining shear and bending models of deformation and carrying out a comparative study of the above two models. Table 2-2 summarizes previous research work on analytical models of blanking force. A brief description of the above models is described in the following sections.

Author and year	Assumptions	Process parameters considered for deriving blanking force
Ramaekers, 1970 and 1986	Pure shear	Ultimate tensile strength, strain hardening component
Atkins, 1980	Pure shear and plain strain	Clearance, strain hardening component, friction factor and strength coefficient
Zhou and Wierzbicki, 1996	Pure tension	Strength coefficient, strain hardening exponent and shear angle
Klingenberg and Singh, 2004	Pure shear and pure tension	Strength coefficient, strain hardening component, clearance, punch penetration

Table 2-2 Previous research work on analytical models for blanking force.

2.2.1 Ramaekers Model [1970]

Ramaekers obtained a simple expression for shear force by assuming a relationship between shear strength (τ) and ultimate tensile strength (σ_{uts}). The proportional factor (S_f) was obtained empirically from micro hardness test in terms of work hardening index (n) as shown below;

$$S_f = \sqrt{\frac{1}{3}\left(\frac{3}{n}\right)^n} \qquad (2\text{-}1)$$

Shear force, F, was approximated using the following equation:

$$F = A_s \tau = (\pi D_p h_0) \times (\sigma_{uts} S_f) \quad (2\text{-}2)$$

where D_p = Punch diameter

σ_{uts} = Ultimate tensile strength

h_0 = Sheet thickness

S_f = Proportional factor

This approach is limited to the calculation of maximum shear force but not the force evolution.

2.2.2 Atkins Model [1980]

Atkins assumed a pure shear model and a plain strain condition for the blanking/piercing process and proposed the geometry shown in Figure 2-2. The main disadvantage of Atkins model is that it assumes only pure shear and the existence of compressive and tensile forces are not considered. Atkins model is purely geometry dependent, regardless of clearance and punch edge radius.

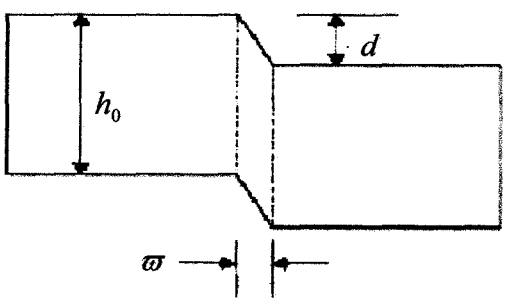

Figure 2-2 Geometry of Atkins model [Atkins, 1980].

Atkins proposed the following formula for the blanking force with friction *f* modeled through an assumed proportion of the shear stress. Shear force F is expressed as:

$$F = \pi D_p \tau [(h_0 - d) + 2fd] \tag{2-3}$$

with $$\tau = C_1 \gamma^n \tag{2-4}$$

where D_p = Punch diameter

τ = Shear stress

h_0 = Sheet thickness

d = Punch displacement

f = Coefficient of friction

C_1 = Material constant

γ = Shear strain

By differentiating equation (2-3) with respect to punch displacement, punch penetration (*d*) and shear strain (γ) at maximum force were obtained as:

$$d_{peak} = \frac{n}{(1+n)(1-2f)} \times h_0 \tag{2-5}$$

$$\gamma_{peak} = \frac{n}{(1+n)(1-2f)} \times \frac{h_0}{\varpi} \tag{2-6}$$

where ϖ is the clearance between punch and die.

2.2.3 Zhou and Wierzbicki Model [1996]

Zhou and Wierzbicki viewed the blanking/piercing process as essentially a purely tensile operation, whereby the fibers surrounding the hole are stretched according to a certain assumed geometry. The base assumption is shown in Figure 2-3.

An assumption that large rotation of material caused by tension exists in the shear zone was made to estimate the plastic behavior and to further calculate the shear force, plastic work and the shape of shear zone.

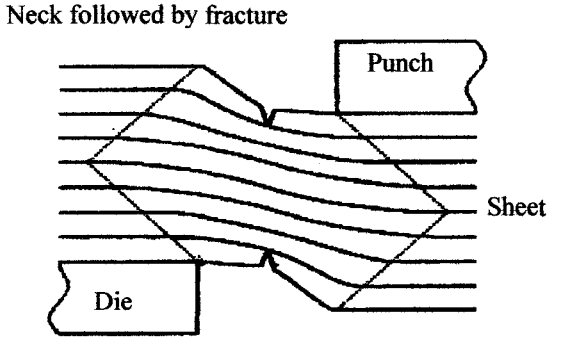

Figure 2-3 Geometry of Zhou et. al model [Zhou and Wierzbicki, 1996].

The shear force was calculated using power law for material hardening as follows:

$$Q = \int dQ = 2\left(\frac{2}{\sqrt{3}}\right)^{n+1} \cdot \frac{Ku}{\zeta} I_m \qquad (2\text{-}7)$$

where Q = Shear force

K = Strength coefficient

I_m = Correction factor

u = Punch displacement

ζ = Displacement function

n = Strain hardening exponent

The correction factor I_m is expressed as a function of material rotation (shear) angle γ and displacement function ζ as follows:

$$I_m = \int_{\gamma_0}^{\gamma_f} \left(\ln\sqrt{1+\gamma^2}\right)^n \frac{1}{\gamma\left(1+\gamma^2\right)} \left(1+\frac{\zeta.\gamma\sqrt{1+\gamma^2}}{4\ln\sqrt{1+\gamma^2}}\right)^n d\gamma \qquad (2\text{-}8)$$

where γ_0 and γ_f are limits of integration. Differentiating equation (2-7) and using $\left(dQ/d\gamma = 0\right)$ gives the following condition for obtaining the maximum shearing force:

$$n = \frac{\gamma_c^{\,2}-1}{\gamma_c^{\,2}} \ln\sqrt{1+\gamma_c^{\,2}} \qquad (2\text{-}9)$$

Shear strain (γ_c) is derived as a function of material work hardening index (n).

2.2.4 Klingenberg and Singh Model [2004]

Klingenberg and Singh compared and expanded the models proposed by Atkins [Atkins, 1980] and Zhou and Wierzbicki [Zhou and Wierzbicki, 1996]. Klingenberg et al. proposed a model with pure shear combined with bending as shown in Figure 2-4, which is still a simplified representation of the actual process.

(a)

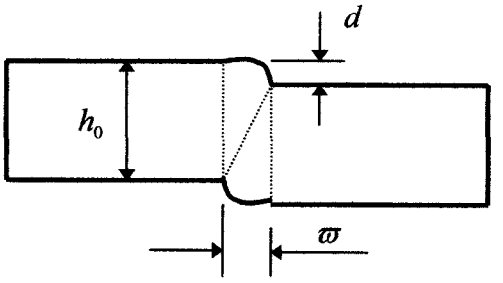

(b)

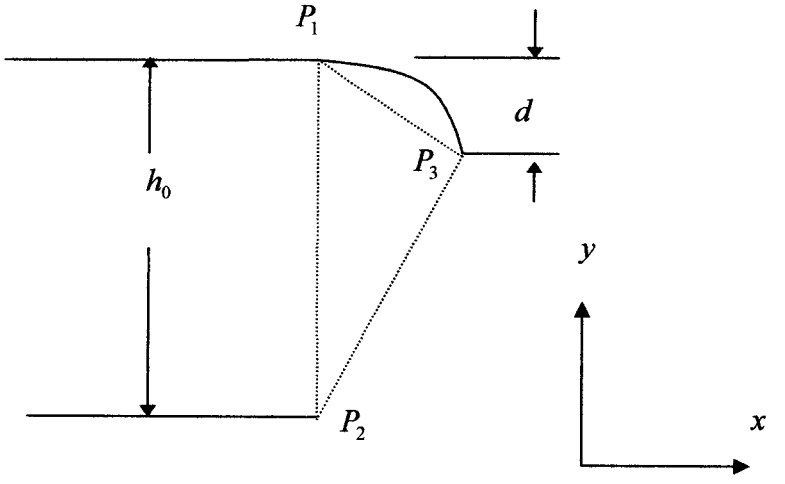

(c)

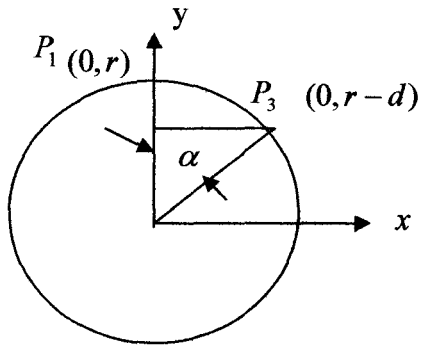

Figure 2-4 Geometry of Klingenberg and Singh model (a) pure shear with bending, (b) Enlarged bending of the blank and (c) Enlarged geometry of bend radius (r).

It was assumed that as the punch penetrates the blank, the additional strain due to curvature increase develops into a circular section shown in Figure 2-4 (c). After setting the slope of curvature at P_2 equal to zero and using the coordinates of the points P_2 and P_3, the radius follows from the geometry of the circle as:

$$r = \frac{\varpi^2 + d^2}{2d} \tag{2-10}$$

whereas, the angle α is given by: $\tan\alpha = \frac{\varpi}{r-d}$ (2-11)

Klingenberg et al. proposed the following equation for the blanking force:

$$F(d) = \psi(d) \cdot F_{shear}(d) \qquad (2\text{-}12)$$

where

$\psi(d)$ is a factor to allow for bending which is a function of punch penetration.

F_{shear} is the punch force considering pure shear as proposed by Atkins.

By considering friction as negligible in blanking, Equation (2-12) was written for a round hole piercing/blanking as:

$$F_{blanking} = \psi(d) \cdot \pi D_p \tau (h_0 - d) \qquad (2\text{-}13)\ (a)$$

where $\psi(d) = k(d)^n$ (2-13) (b)

where, $k(d)$ is the factor by which principal strain is multiplied to arrive at the value adapted for bending and given as:

$$d \le \omega: \quad k(d) = \frac{\ln\left(\frac{\alpha r}{\omega}\right)}{\ln\sqrt{1+\gamma^2}} \qquad (2\text{-}14)\ (a)$$

$$d > \omega: \quad k(d) = \frac{\ln\left(\frac{1}{2}\pi + \gamma - 1\right)}{\ln\sqrt{1+\gamma^2}} \qquad (2\text{-}14)\ (b)$$

and $\tau = C_1 \gamma^n$ (2-15)

where C_1 is a work hardening factor.

Assuming work hardening occurs according to simple power law, vonMises expression for equivalent stress and strain can be adopted for an assumed pure shear situation as follows:

$$\bar{\sigma} = C_2 \bar{\varepsilon}^{n} \tag{2-16}$$

$$\tau = \frac{\bar{\sigma}}{\sqrt{3}} \tag{2-17}$$

$$\bar{\varepsilon} = \frac{\gamma}{\sqrt{3}} \tag{2-18}$$

The constant C_1 in Equation (2-15) and C_2 in Equation (2-16) are related by:

$$C_1 = \frac{C_2}{\left(\sqrt{3}\right)^{n+1}} \tag{2-19}$$

Klingenberg et al. used Eq. (2-13) with Eq. (2-14) to (2-19), in order to obtain the blanking force in their new model. Klingenberg et al. further compared the new analytical model against results from finite element analysis and experiments which are shown in the Figure 2-5 and Table 2-3. The model predictions were in good agreement with experimental results and were more accurate at smaller clearances, for conditions in which shearing becomes dominant.

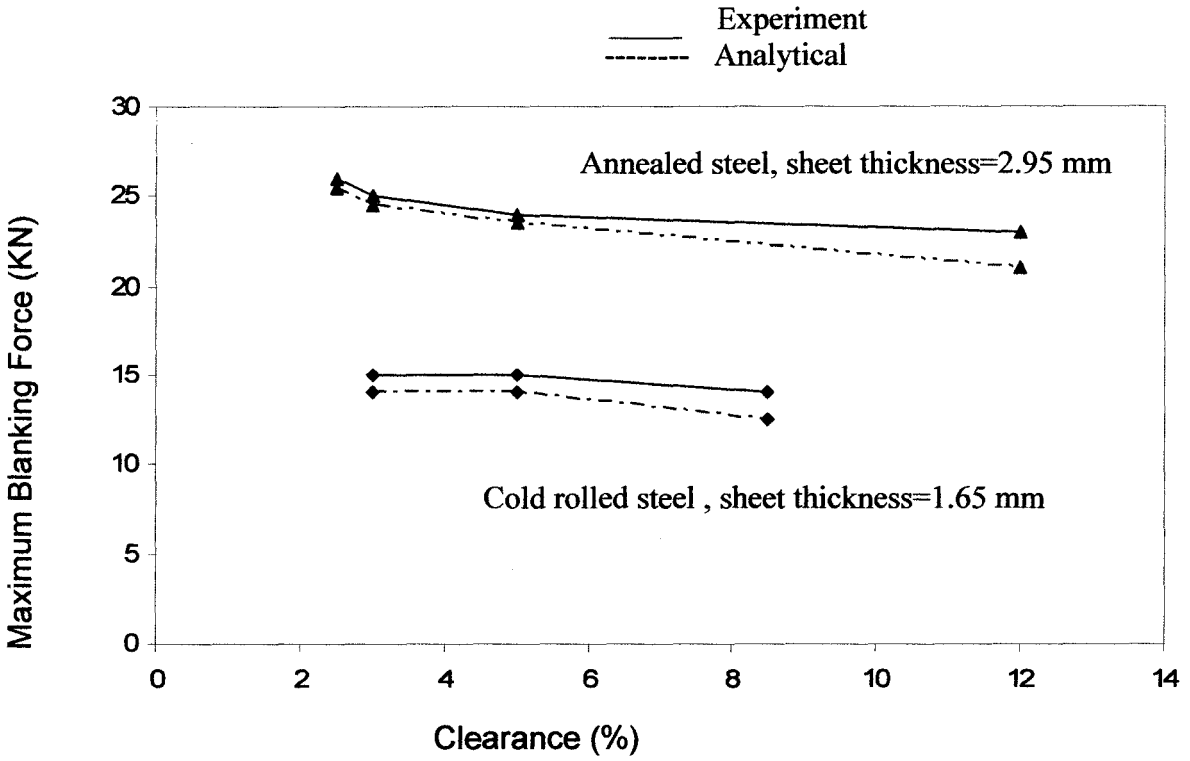

Figure 2-5 Comparison of [Klingenberg and Singh, 2004] model with experimental results.

Material	Experiment	FEM(ABAQUS)	Analytical model
Annealed steel, $h_0 = 2.95$ mm and c=12.2%	22.9	23.2	20.3
Cold rolled steel, $h_0 = 1.6$ mm and c=12.2%	14.3	13.7	12.4

Table 2-3 Values of maximum blanking force (F) for typical clearances, [Klingenberg and Singh, 2004].

2.3 Tool Wear Models

The tool wear resulting from abrasive or adhesive wear has been discussed in the previous chapter. Many researchers used the Archard equation [J.F.Archard, 1953] to describe tool wear in metal stamping. A simplified expression for the volume of abrasive wear is given as:

$$w = \frac{V}{s} = k\frac{F}{3H} \tag{2-20}$$

where,

w = Wear rate or worn volume per unit sliding distance

V = Volume of material removed by wear from punch surface

s = Sliding distance

k = Wear coefficient

F = Normal load applied on punch

H = Hardness of the punch material

The wear coefficient k is dependent upon stamping conditions including tool and sheet material properties, die clearance, sliding speed, friction and lubrication. The value k can be found only through experiments. The wear resistance of tool steels is not simply a matter of hardness. Maeda and Aoki [

Maeda and Aoki, 1975] heat treated a 12% Cr steel (similar to AISI D2 steel), a high speed steel (M2), and a low alloy steel (O2) to a common hardness of 61 HRc and bainitic steel sheets in hardness ranging from 290 to 440 VHN were punched. Face wear, which is due mostly to abrasion, was least with D2, greater with M2, and greatest with O2.

It was stated that Rockwell hardness is an inadequate measure of wear resistance, essentially because it measures only the matrix hardness H_m, whereas resistance to wear is affected also by the hardness of the dispersed (carbide) phase H_c, which occupies an area α. An effective hardness H_{ve}, can be calculated using the following 'rule of mixture' expression:

$$H_{ve} = H_c + (1-\alpha)H_m \qquad (2\text{-}21)$$

Bourithis et al, [Bourithis, 2005] compared the wear resistance of two commercial cold steels AISI D2 and O1 using pin abrasion tests. Both tool steels were heat treated to exactly the same hardness of 700 HV. The volume loss with respect to sliding distance at different loads was measured. The result was consistent with Archard wear Eq 2-20 as shown in Figure 2-6. For both tool steels, the wear rate increased linearly with the applied load. Based on normalized wear rates for both tool steels, it was found that D2 steel performed two times better than O1 even though they were heat treated to the same

hardness. The superior performance of D2 steel is due to the blocky carbides in its microstructure, which enhance the wear resistance. The values of normalized wear rate are listed in Table 2-4. The Archard Equation 2-20 has been further modified as:

$$w = K'F \tag{2-22}$$

where K' is defined as normalized wear rate and is the slope of the line (Figure 2-6).

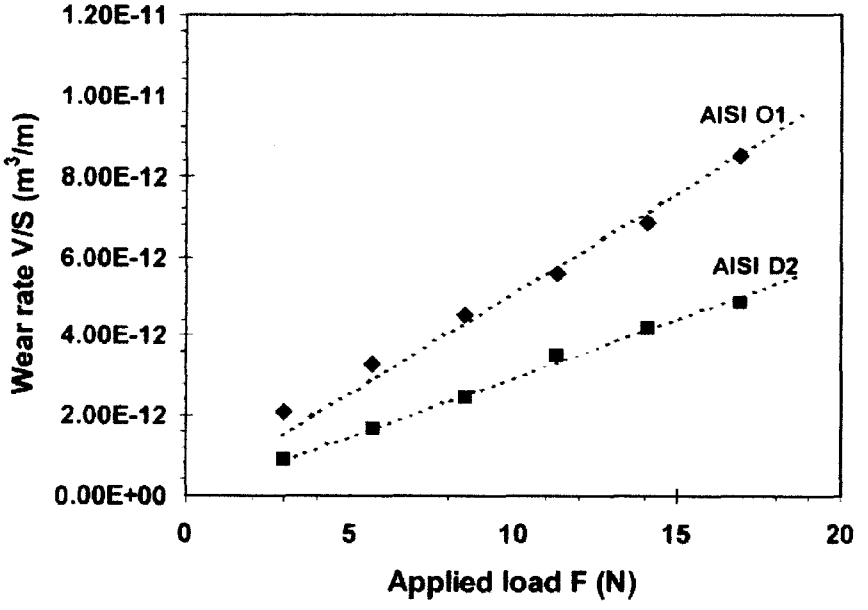

Figure 2-6 Definition of normalized wear rate [Bourithis, 2005].

Tool steel	Hardness (HV)	K' (m^3/Nm)	Reference
AISI O_1	700	$1.88 \pm 0.08X10^{-13}$	[Bourithis,2005]
AISI D_2	700	$1.01 \pm 0.07X10^{-13}$	[Bourithis,2005]
AISI M_2	715	$1.21 \pm 0.3X10^{-13}$	[Navas ,2005]

Table 2-4 Normalized wear rate K' for different tool materials.

Navas et al, [Navas, 2005] compared the wear resistance of tool steels with AISI M2 and AISI 431. The experimental results were in agreement with Archard wear equation. The AISI M2 showed greater wear resistance than AISI 431 tool steel due to carbides in its microstructure.

2.4 Punch Wear and Tool Life Prediction Models

It is well understood that the product quality deteriorates as tool wear proceeds. From the production point of view, it is economical to produce as many pieces as possible before re-sharpening or replacement of the tool. Thus minimizing the cost of tool re-sharpening or replacement and press downtime involves optimizing the stamping process. This involves prediction of tool, work piece geometry and subsequently establishment of tool re-sharpening schedule in advance. Table 2-5 summarizes some of the previous research work on punch wear and tool life models and a brief description of the same are described in the following sections.

Author, year	Method	Input parameters					Output parameters			
		k	n	f	ω	K'	R_{wp}	b	N	Shear Edge
Taupin, 1996	FEM	Yes	Yes	-	Yes	No	No	Yes	No	No
Dae-Cheol Ko, 2000	FEM	Yes	Yes	Yes	Yes	Yes	Yes	Yes	Yes	Yes
Hambli, 2001	FEM	Yes	Yes	Yes	Yes	Yes	Yes	Yes	No	No
Hambli, 2002	NNW	Yes	Yes	Yes	Yes	Yes	Yes	Yes	No	No
Hambli, 2003	FEM	Yes	Yes	Yes	Yes	Yes	Yes	Yes	Yes	Yes

Table 2-5 Representative tool life and tool wear prediction models.

2.4.1 Taupin et al. [1996] Tool Life Model

Taupin et al. [Taupin, 1996] have developed a FEM model using DEFORM-2D software to predict ductile fracture and burr height. It was assumed that the material has to absorb certain energy first, which was referred to as critical damage value, before fracture initiates. The critical damage value was calculated and used in the FEM model. The process parameters including die clearance and material properties were used in the model to obtain burr height to predict tool life. The burr height from the experiments was compared with FEM results and was found to be in good agreement.

The proposed model does not calculate the tool life in terms of number of parts that can be produced considering punch wear. In addition, the punch material properties such as hardness (H) or wear rate (w) were not taken into consideration in the proposed model.

2.4.2 Dae-Cheol Ko et al. Tool Life Model [2000]

Dae-Cheol Ko, [Dae-Cheol Ko et al. 2000] has also developed a finite element scheme for the prediction of the tool wear. In order to predict tool wear, Archard's wear model was reformulated in an incremental form and then the wear depth on the tool was calculated at each step in the deformation using the result of finite element analysis, taking consideration of the sliding velocity and normal pressure as shown in Equation (2-23).

$$\delta w = \frac{k}{H}\int_0^T \sigma_n \Delta v dt \qquad (2\text{-}23)$$

where

σ_n = Normal stress acting on tool surface

Δv = Sliding velocity between tool and workpiece

T = Total time of deformation

δw = Wear depth

K = Wear coefficient

H = Tool Hardness

The wear coefficient was estimated experimentally by using pin-on-disk method. The measurement of burr height was used to predict tool life. The results from the experimental and numerical analysis were in good agreement as shown in Figure 2-7. The burr height measurement technique was not explained in the detail which is very critical for the specified value of 4 to 7 micrometers.

(a) (b)

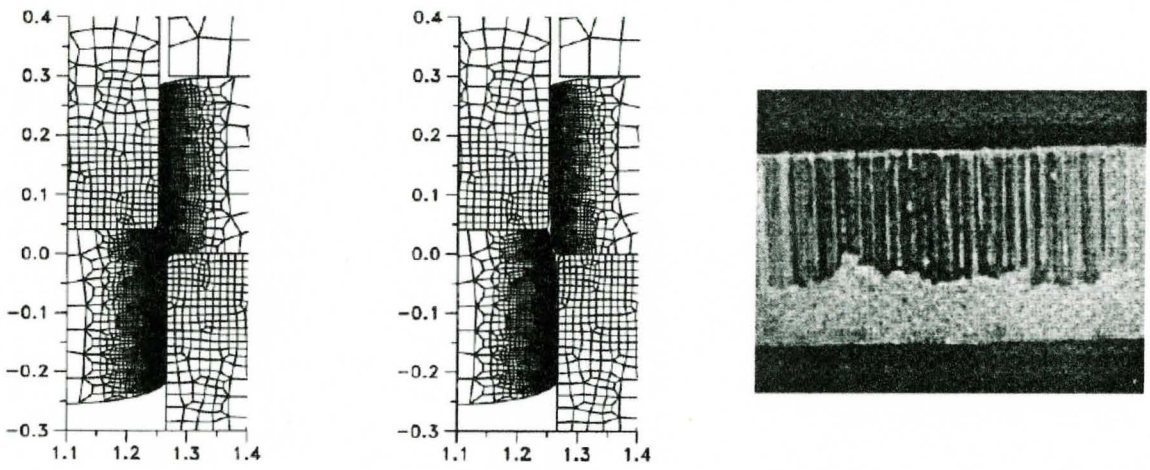

Figure 2-7 Comparison of (a) FEM and (b) experimental results using AISI 4340 as workpiece material [Dae-Cheol Ko et al,

2.4.3 Hambli Tool Life Models [2001, 2002 and 2003]

Most comprehensive models for punch wear and tool life predictions have been developed by Hambli [2001, 2002 and 2003] while considering mainly burr height and punch edge radius as tool life prediction factors in his studies.

As a first step, tool edge radius over time was obtained using the wear model as shown below in Equation 2-24 combined with a FE blanking model. The geometry of the cutting edge is shown in Figure. 2-8. In the second step, tool edge radius was used to predict burr height using FEA. Hambli defined volume of wear resulting from adhesive wear as:

$$V = \frac{5\pi}{4}\left(R_{wp}\right)^3 + \frac{3\pi}{2} R_p \left(R_{wp}\right)^2 = \sum_{i=1}^{n} K_{us} F\, s \qquad (2\text{-}24)$$

where, V = Volume of wear

R_{wp} = Punch edge radius

R_p = Punch radius

F = Normal force on the punch

K_{us} = wear coefficient

n = Total number of blanking cycles

and, sliding length s is given by:

$$s = t \times \frac{H_1}{100} \tag{2-25}$$

where t is the sheet thickness and H_1 is the depth of sheared edge.

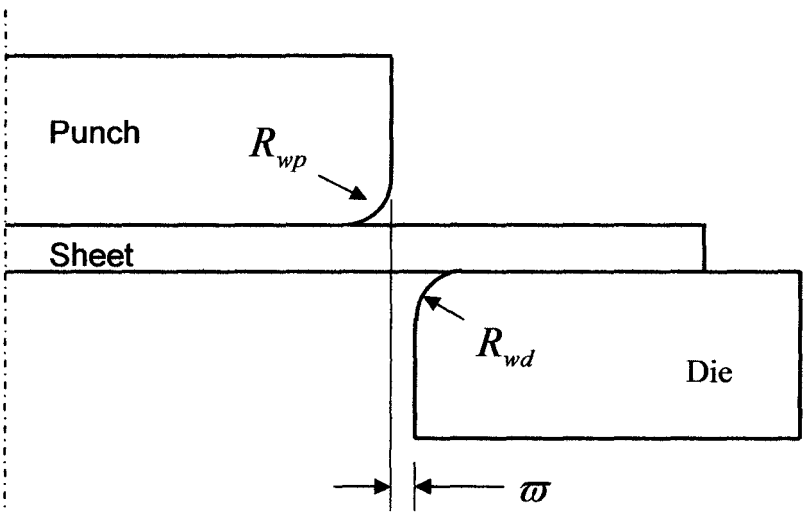

Figure 2-8 Geometry of the cutting edge [Hambli, 2002].

The results obtained are shown in Figure 2-9 and 2-10. The model predictions were in good agreement with experimental results. It was found that the burr height increased linearly with increase in punch edge radius.

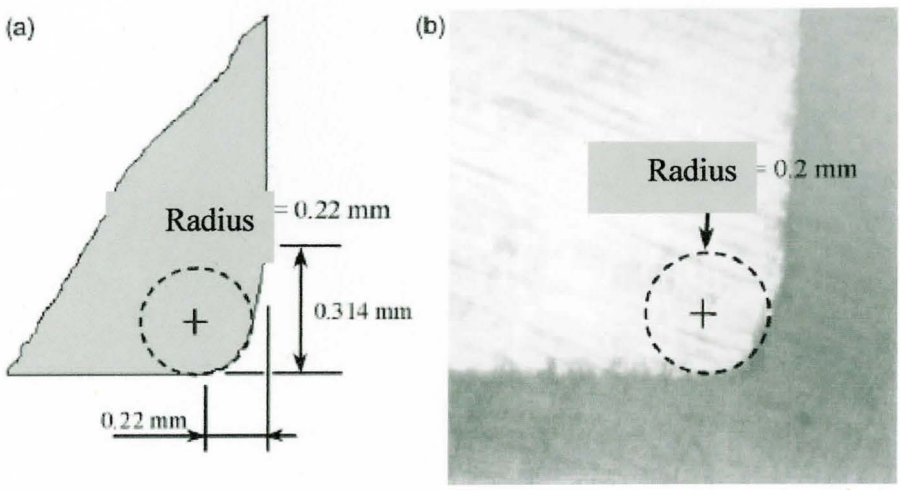

Figure 2-9 Wear profile after 20,000 cycles (a) FEM and (b) Experiment [Hambli, 2002].

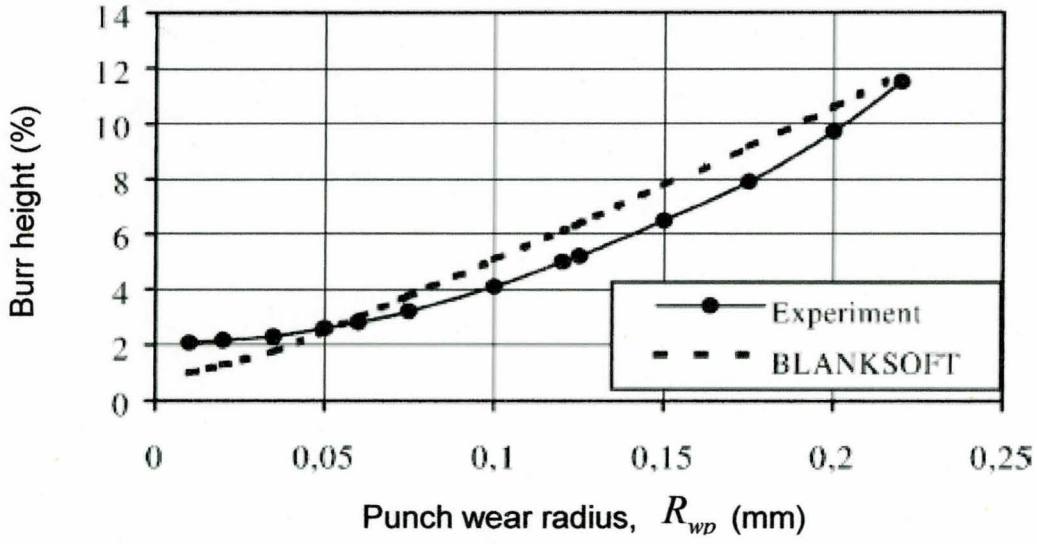

Figure 2-10 Burr height results from FEM and Experiment [Hambli, 2003].

2.5 Comparison of Tool Life Models

Most of the tool life studies discussed in the above sections have shown that the burr height (*b*) increases linearly with punch edge radius (R_{wp}), whereas mixed results have been reported on burr height with reference to die clearance (ϖ) (Fig. 2-11).

A study by Hatanaka [Hatanaka, 2003] has shown that the burr height decreased at the lower clearance value up to 10% whereas the clearance increased gradually in another study by Hambli [Hambli, 2002]. It is also to be noted that burr height was changed in a zigzag manner in another study by Rachik [Rachik, 2002].

In general, the burr height is acceptable up to 10% of sheet thickness and is measured in micrometers. One reason for getting mixed results could be the errors in measurement of burr height. The measurement technique used to measure burr height was mostly conventional and it suggests that there is a need to evaluate a suitable method of measurement in order to reduce error. The burr height also varies from type of die used to produce the part. Most of the precision parts are manufactured using progressive dies and few parts are made by compound dies or single station dies. The burr on a part generated by a single station blanking die is different than a progressive die. Blank is pushed or ejected in a single station die; whereas, part is formed at the final stage in a progressive

die while it undergoes several cutting, forming and bending operations at individual stations. Stripper acts as a blank holder and exerts about 10 to 15% of total force involved in a progressive die.

The burr formed in a piercing/notching station gets flattened by the stripper at each station and until the final station. This process of burr flattening will reduce the amount of burr height on the final part in the progressive die. The burr will get reduced further during the secondary operations like heat treatment and deburring of the parts. This is the limitation of burr measurement in progressive dies to correlate tool life with reference to burr height. Hence, measurement of burr on the final part produced using a progressive die doesn't reflect the actual burr height, thereby, a different technique is needed to measure burr height accurately in the progressive dies if tool life has to be defined using burr height.

On the other hand, the burr on slugs produced during the notching/piercing operations does not undergo this kind of flattening or deformation in progressive dies. The burr height on slugs could be taken as a reference for burr formation on the part whereas the actual burr on the part might not be equal to it. More importantly, a proper technique of burr height measurement also plays a vital role. A suitable method for burr height measurement has been developed in the present work.

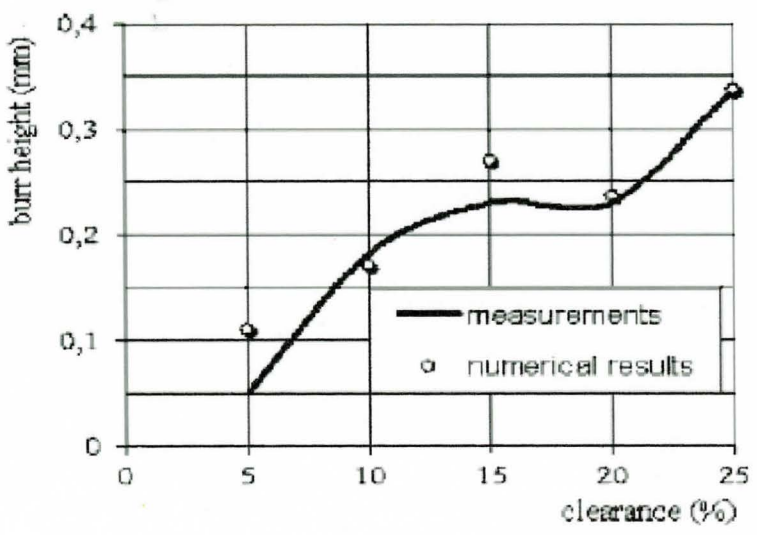

(a)

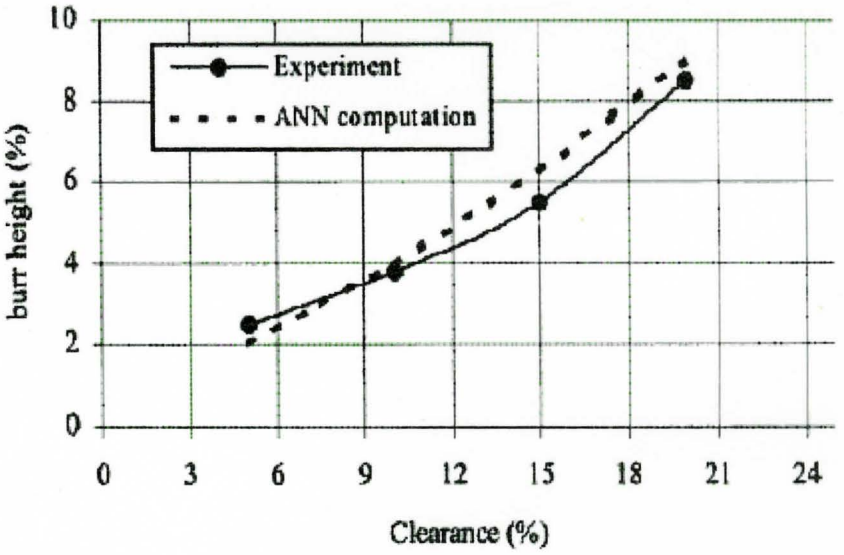

(b)

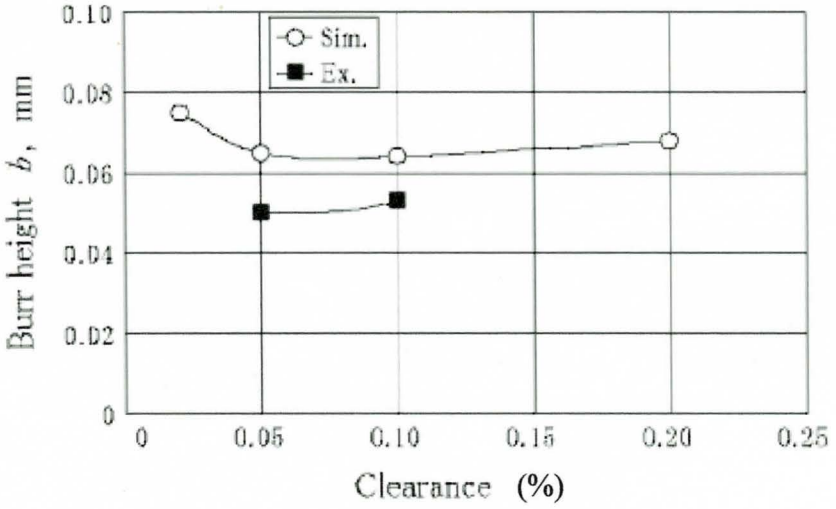

(c)

Figure 2-11 Mixed results on burr height versus clearance (a) Rachik [2002], (b) Hambli [2002] and (c) Hatanaka [2003].

2.6 Need for an Analytical Tool Wear Model to Predict Tool Life in Stamping Dies

With the development of finite element models of tool wear to predict tool life by various researchers, important possibilities emerged to model and analyze the process in a research environment. However, FE models are less well suited for use in a production environment. For real-time monitoring of tool wear and tool life, an analytical model could potentially be more efficient and useful.

On the other hand, prediction of burr height is used as a main factor to determine tool life in the various research studies as explained in the previous sections. Whereas, tool life in precision stampings is mostly defined either in terms of part dimensions or burr height, whichever exceeds the tolerance limit as discussed in Section 1.2.4. As the size of the hole is a critical factor in precision parts, a study on hole size variation due to tool wear, with an aim to derive an equation to predict tool life in terms of number of parts, is very useful.

In the next chapter, an attempt has been made to derive a new analytical model for tool life in metal stampings using punch and sheet material properties.

Chapter 3

Proposed Model for Tool Life

3.1 Tool Life Prediction Based on Modified Wear Equation

Let us consider that a punch is used to pierce a hole in a sheet as shown in Fig. 3-1 and the punch is subjected to abrasive wear as discussed earlier in chapters 1 and 2.

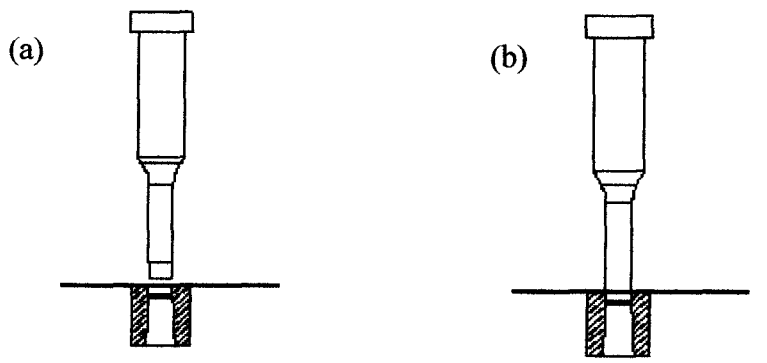

Figure 3-1 Punch and die elements in (a) open and (b) closed configurations.

The punch wear is defined by Archard wear equation (Section 2.3 and Equation 2-20) as:

$$w = \frac{V}{s} = k\frac{F}{3H} = K'F \qquad (3\text{-}1)$$

Assuming the wear rate is constant for maximum punch force, the punch wears by area w for each punch stroke and it produces a variable hole size in the part. If A is the initial area of the punch, the wear pattern of punch area can be described as follows:

For stroke 0, the punch area is A

1, A - w

2, A - $2w$

3, A - $3w$

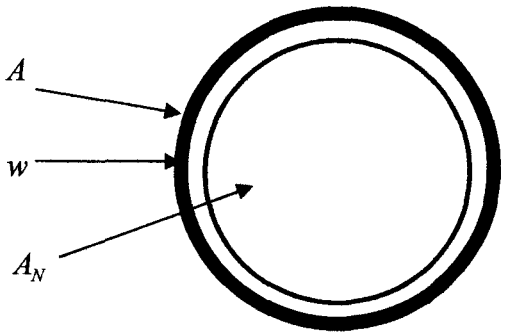

Figure 3-2 Punch wear pattern.

The above pattern shows that the wear behavior and the resultant punch size variation follow an arithmetic progression with a common difference of w. Hence, punch area (A_N) after N number of punch strokes (Fig. 3-2) can be defined by the n^{th} term in the arithmetic progression as:

$$A_N = A - (N.w) \tag{3-2}$$

From Equation (3-2), number of punch strokes (N) required for the punch to wear from the initial punch area A to reduced area A_N, can be written as;

$$N = \frac{(A - A_N)}{w} \tag{3-3}$$

By substituting Eq. (3-1) in (3-3) for wear area w *(mm² per stroke)*

$$N = \frac{(A - A_N)}{K'F} \tag{3-4}$$

While using the Equation (3-4) and assuming punch pierces same size hole on the part , one can find the number of parts (N) that could be stamped between the initial hole size (A) and the allowed hole size (A_N) after wear. Following conclusions can be drawn from the above new tool life model:

- The initial punch area (A) and the allowable area (A_N) after the punch wear for a given shape and size can be obtained by the size and tolerance specified on the part. Hence tool life can be defined in terms of number parts between two re-sharpenings for a given piercing hole size and tolerance.

- Number of parts (N), that can be stamped, is inversely proportional to the force (F) exerted on the punch in the blanking/piercing.

The determination of parameters used in the new tool life model, Eq. (3-4), for different hole shapes, blanking force and normalized wear rate are discussed in the following sections. The normalized wear rate of the punch is assumed as constant for a given punch material.

3.1.1 Geometry of Pierced Holes and Effect of Tool Wear

Generally, the geometry of the most used piercing operations is circular. Often, square and rectangular holes are also pierced for the assembly of bolts and nuts.

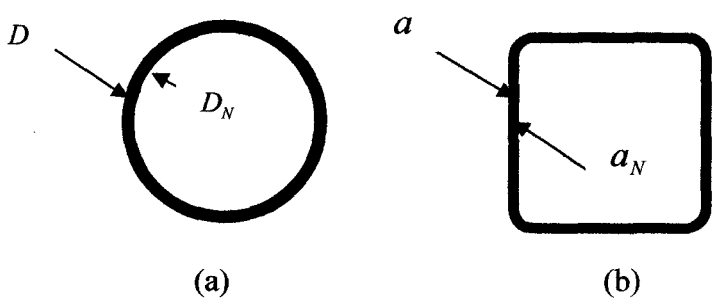

Figure 3-3 Geometry of piercing punches (a) circular and (b) square shapes.

Two types of piercing punch profiles are studied in the present work as listed in Figure 3-3 and Table 3-1.

	Shear length L	New punch area (A)	Worn punch area (A_N)
Circular	πD	$\frac{1}{4}\pi(D^2)$	$\frac{1}{4}\pi(D_N{}^2)$
Square	$4a$	a^2	$a_N{}^2$

Table 3-1 Profiles of punch geometry.

For a circular hole, the tool life Equation (3-4), using Table 3-1, can be expressed as:

$$N = \frac{\pi}{4}\frac{\left(D^2 - D_N{}^2\right)}{K'F} \tag{3-5}$$

For example, if the part has a hole having dimension $\phi 5.00^{\pm 0.05}\,mm$:

D = 5.05 mm, will be the initial punch diameter;

D_N = 4.95 mm, will be the allowed punch diameter after wear;

Similarly, the tool life for a square hole having side a, can be given as:

$$N = \frac{\left(a^2 - a_N{}^2\right)}{K'F} \tag{3-6}$$

where, a = Initial length of side of the square;

and a_N = Allowed length of side of the square, after wear;

In general, areas of any given profile can be studied using this concept.

3.1.2 Determination of Normal Force (F)

The normal force defined in Equation (3-1) is equal to the maximum blanking/piercing force discussed earlier in Section 2.2. In this section, four different models are discussed for the determination of normal force. Assuming precision stampings where the punch and die clearance is below 10% of sheet thickness, the Equation (2-12) from Klingenberg at al. appears to be most promising and is adapted here. Therefore, Equation (2-12) is used in Equation (3-1) to determine the blanking force as follows:

$$F = \psi(d).F_{shear}(d) = \psi(d)L\tau(h_0 - d) \qquad (3\text{-}7)$$

where τ is shear stress, h_0 is sheet thickness, d is punch penetration depth and L is length of cut in blanking/piercing which changes from shape to shape of the notch contour. The shear length (L) for a circular and square hole was given earlier in Table 3-1.

The above model accounts for pure shear, bending, process and material parameters including sheet thickness, strain hardening index, shear strain, depth of punch penetration, die clearance, roll over radius and bending factor as summarized below in Table 3-2.

Parameter name	Equation	Symbols
Peak punch penetration	$d = \frac{n}{(1+n)(1-2f)} \times h_0$	n = Strain hardening index f = Friction coefficient ϖ = Die clearance C_2 = Strength coefficient h_0 = Sheet thickness
Bend angle	$\tan\alpha = \frac{\varpi}{r-d}$	
Bend radius	$r = \frac{\varpi^2 + d^2}{2d}$	
Work hardening factor	$C_1 = \frac{C_2}{\left(\sqrt{3}\right)^{n+1}}$	
Peak strain	$\gamma = \frac{n}{(1+n)(1-2f)} \times \frac{h_0}{\varpi}$	
Shear stress	$\tau = C_1 \gamma^n$	
Bending factor	$\psi(d) = (k(d))^n$	
Principle strain factor	$d \le \varpi;\ k(d) = \frac{\ln\left(\frac{\alpha r}{\varpi}\right)}{\ln\sqrt{1+\gamma^2}}$ $d > \varpi;\ k(d) = \frac{\ln\left(\frac{1}{2}\pi + \gamma - 1\right)}{\ln\sqrt{1+\gamma^2}}$	

Table 3-2 List of parameters used in the blanking force model.

The second option for blanking force may be taken from Ramaeker's model discussed in the Section 2.2.1 and Equation (2-2) as:

$$F = Lh_0\sigma_{uts}S_f \tag{3-8}$$

This is a simple model which can be used for calculating normal force (F) using ultimate tensile strength (σ_{uts}) of the sheet material and a proportion factor (S_f) between shear strength and ultimate tensile strength.

3.1.3 Final Tool Life Prediction Using Punch Wear Models

For a circular hole, the tool life in terms of number of parts for a given tolerance can be obtained by substituting blanking force Equations (3-7) and (3-8) in equation (3-5).

Tool life model- 1:

Using Equation (3-7) in (3-5) gives:

$$N = \frac{\pi}{4K'} \times \frac{\left(D_p{}^2 - D_N{}^2\right)}{\psi(d)L\tau(h_0 - d)} \tag{3-9}$$

Tool life model- 2:

Using Equation (3-8) in (3-5) gives:

$$N = \frac{\pi}{4K'} \times \frac{\left(D_p{}^2 - D_N{}^2\right)}{Lh_0\sigma_{uts}S_f} \tag{3-10}$$

For a square hole, tool life can be obtained by substituting blanking force Eq (3-7) and (3-8) in (3-6).

Tool life model- 3:

Using Equation (3-7) in (3-6) gives:

$$N = \frac{1}{K'} \frac{\left(a_p{}^2 - a_N{}^2\right)}{\psi(d)L\tau(h_0 - d)} \tag{3-11}$$

Tool life model- 4:

Using Equation (3-8) in (3-6) gives:

$$N = \frac{1}{K'} \times \frac{\left(a_p{}^2 - a_N{}^2\right)}{Lh_0\sigma_{uts}S_f} \tag{3-12}$$

The proposed Equations (3-9) and (3-10) for a round punch are tested and analyzed in the next chapter to obtain a better model.

3.1.4 Tool life model using piercing hole size

Assuming that the size of the pierced hole is equal to the punch. It is also possible to find out the hole size reduction due to punch wear with respect to number of punch strokes/parts. For a round hole, the Equation (3-5) can be written as;

$$D_N = \sqrt{(D^2 - \frac{4}{\pi} NK'F)} \tag{3-13}$$

This model can be verified by finding and comparing the hole size on the part from the experiment as discussed in the next chapter. The above Equation (3-13) is quite general and can be applied to any hole profile.

3.1.5 Determination of Punch Normalized Wear Rate in Abrasion (K')

The normalized abrasive wear rate is expressed from equation (3-1) as:

$$K' = \frac{V}{Fs} \tag{3-14}$$

The volume loss (V) of the punch can be found experimentally by measuring the punch weight before and after stamping as:

$$V = \frac{m - m_N}{\rho} \tag{3-15}$$

where m = Punch weight before stamping

m_N = Punch weight after N number of punching operations

ρ = Density of punch material

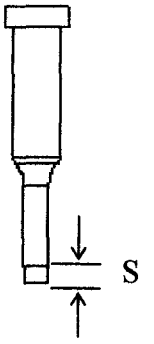

Figure 3-4 Punch sliding length (S).

If punch sliding length for every stroke is S, then total sliding distance (s) after N number of punching operations (Fig. 3-4) can be defined as:

$$s = SN \tag{3-16}$$

By combining Eq. (3-14), (3-15) and (3-16), we can obtain normalized wear rate in abrasion as:

$$K' = \frac{(m - m_N)}{\rho SNF} \tag{3-17}$$

Normal force (F) can be defined from Eq. (3-7) or (3-8). Normalized wear rate (K') can be found using Eq. (3-17) for a given stamping condition.

3.2 Tool Life Prediction Based on Burr Height

Let us assume that the punch and die clearance (ϖ) is set to an optimum value according to the required cutting edge quality and punches are sharpened to the minimum edge radius (R) at the beginning of production (Fig. 3-5)

Let $f(x)$ be the burr height at the beginning of punching which is primarily dependent on the initial clearance and punch edge radius. Therefore;

$$f(x) \propto (\varpi + R) \tag{3-18) (a}$$

The punch edge radius starts increasing due to punch wear (Fig. 3-5), which in turn increases the burr (in addition to the initial burr $f(x)$). Many studies have found that the burr height increases linearly with punch edge radius and is approximately considered as equal to the punch edge radius.

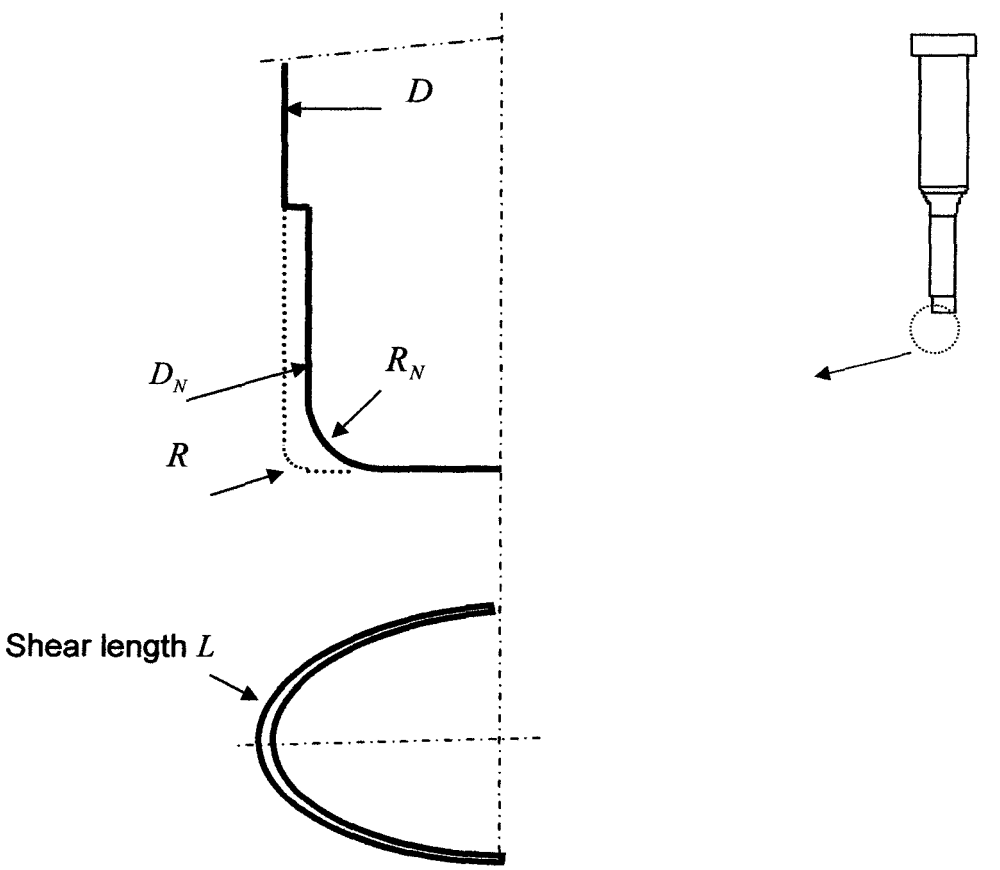

Figure 3-5 Enlarged view of punch edge wear
(Half section with plan and elevation).

Accordingly, additional burr height, $f(y)$, is due to increased edge radius (R_N), can be written as:

$$f(y) \propto R_N \qquad \text{(3-18) (b)}$$

Hence, the total burr height (b) during stamping can be defined by combining initial burr height $f(x)$ and the burr height due to edge wear $f(y)$ as:

$$b \propto f(x) + f(y) \qquad \text{(3-19)}$$

Finally, the burr height (b_N) after *N* number of punching strokes using Eq. (3-19) can be written as:

$$b_N \propto (\varpi + R) + R_N \qquad \text{(3-20) (a)}$$

$$\text{or} \quad b_N = C\{(\varpi + R) + R_N\} \qquad \text{(3-20) (b)}$$

where C is a constant, whose value is to be found through experiment.

As per the model in Eq. (3-20), it is possible to calculate the burr height (b_N) during production if the value of edge radius (R_N) is known with reference to the number of punch strokes. The determination of punch edge radius due to punch edge wear is discussed in the next section.

3.2.1 Determination of Punch Edge Radius (R_N)

The punch edge wear is mainly due to adhesive wear and can be determined using Archard's equation as:

$$V_N = sK''F \tag{3-21}$$

where K'' is normalized wear rate due to adhesive wear and *s* is punch sliding distance which is equal to the depth of punch penetration (*d*) (Fig. 2-1) at each punch stroke as:

$$s = Nd \tag{3-22}$$

The punch edge wear volume (V_N) at N number of punch strokes can be calculated using Fig. 3-5 and 3-6 as below:

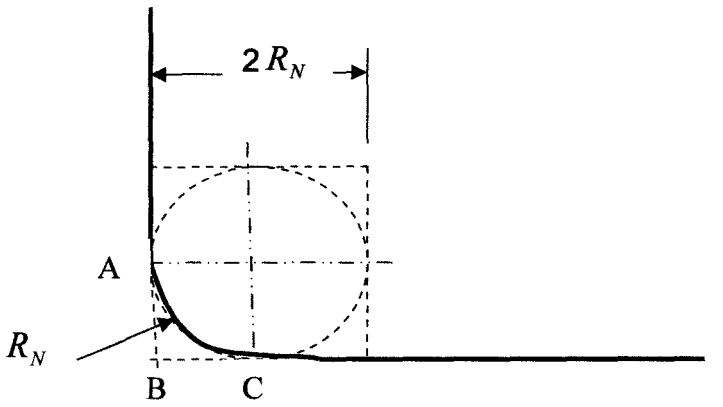

Figure 3-6 Enlarged view of punch edge radius

The punch edge area (ABC) may be calculated using the Fig 3-6 as:

$$\text{Area of ABC} = \frac{1}{4}\,(\text{Area of square} - \text{Area of circle}) \qquad (3\text{-}23)\ (a)$$

$$= \frac{1}{4}\left[\left(4R_N{}^2\right) - \left(\pi R_N{}^2\right)\right] \qquad (3\text{-}23)\ (b)$$

$$= \left(1 - \frac{\pi}{4}\right) R_N{}^2 \qquad (3\text{-}23)\ (c)$$

Finally, the edge wear volume (V_N) using area ABC can be calculated as:

$$V_N = \text{Shear length X Area of ABC} = L\left(1 - \frac{\pi}{4}\right) R_N{}^2 \qquad (3\text{-}24)$$

where L is the shear length as given in Table 3-1.

By combining Equations (3-21), (3-22) and (3-24), the edge radius (R_N) can be calculated as:

$$R_N = \sqrt{\frac{NdK''F}{L\left(1-\frac{\pi}{4}\right)}} \tag{3-25}$$

3.2.2 Final Tool Life Model Based on Burr Height

By substituting Eq. (3-25) in (3-20) (b), the burr height (b_N) at N number of punching strokes can be written as:

Tool life model 5:

$$b_n = C\left[(\varpi + R) + \sqrt{\frac{NdK''F}{L\left(1-\frac{\pi}{4}\right)}}\right] \tag{3-26}$$

The tool life model in Equation (3-20) and (3-26) have been tested experimentally and results are discussed in chapter 4. General trends of the proposed tool life models are further discussed in chapters 5 and 6.

Chapter 4
Experimental Methods and Results

4.1 Production Process

Experiments were conducted at OPPLAST Inc. on a precision part (U-Clip) which has been used in the present research to study the punch wear process to verify the proposed tool life models discussed in the previous chapter. The press used for the experiments was a custom made C-type hydraulic press. The progressive die was mounted on the bed which moved up and down with a maximum speed of 50 strokes per minute. The press was equipped with automatic coil feeder. A photograph of the setup is shown in the Figure 4-1.

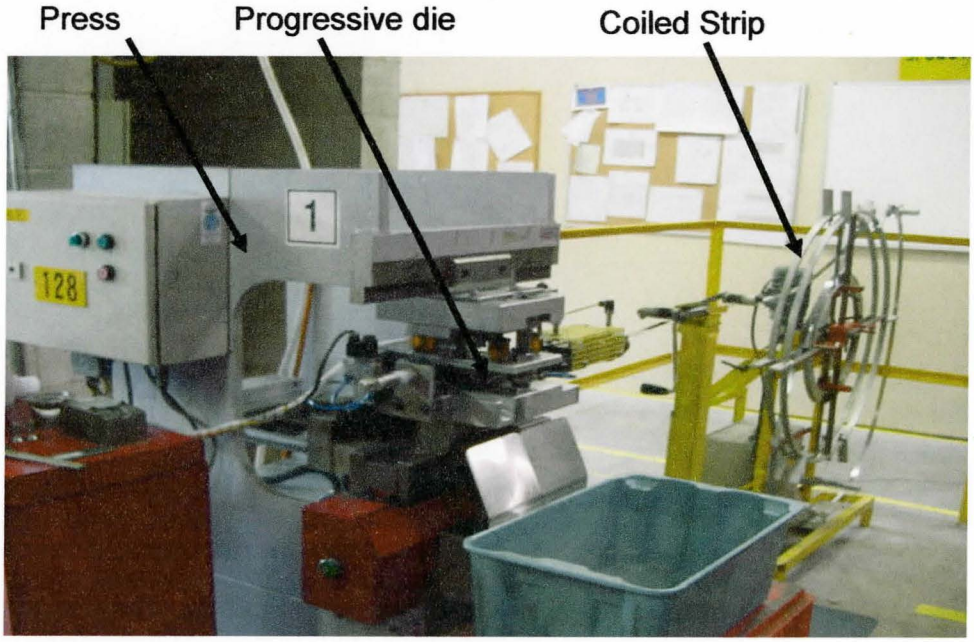

Figure 4-1 Production setup used at OPPLAST Inc.

4.2 Part Details

4.2.1 Part Description

The part produced from the progressive die discussed in Section 4-1, is a U-Clip as shown in Figure 4-2.

(a)

(b)

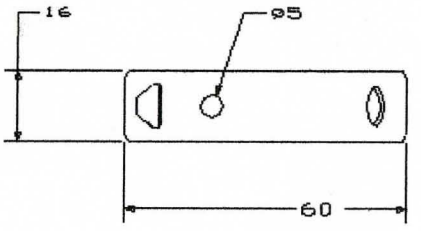

Figure 4-2 Part details (a) final part and (b) blank development (Dimensions are in millimeters.)

4.2.2 Sheet Material Chemical Composition

The sheet material was austenitic stainless steel AISI 301 having material composition as given in Table 4-1.

Material grade	Chemical composition						
	% C	% Si	% Mn	% Cr	% Ni	%P	% S
AISI 301	0.15	1	2	18	8	0.045	0.03

Table 4-1 Sheet material composition (wt %).

4.2.3 Sheet Material Properties

Standard tensile tests were performed to obtain the material properties. The test samples were prepared as per the ASTM E 8M-04 standard and tests were conducted in the Laboratory. The test details are listed in Appendix-A. An average value for 3 replicates is reported in Table 4-2. These material properties are typical of AISI 301 used in stamping.

Material	Thickness (mm)	UTS (MPa)	K (MPa)	n
AISI 301	0.4	1325	1160	0.288

Table 4-2 Sheet material properties from uniaxial tensile test.

4.3 Die Details

4.3.1 Strip Layout

The part was produced using a progressive die as per the strip layout shown in Figure 4-3. A round punch was selected to observe the wear behavior and the details of the punch are listed in Table 4-3. The material composition of the punch material AISI M2 is given in Table 4-4.

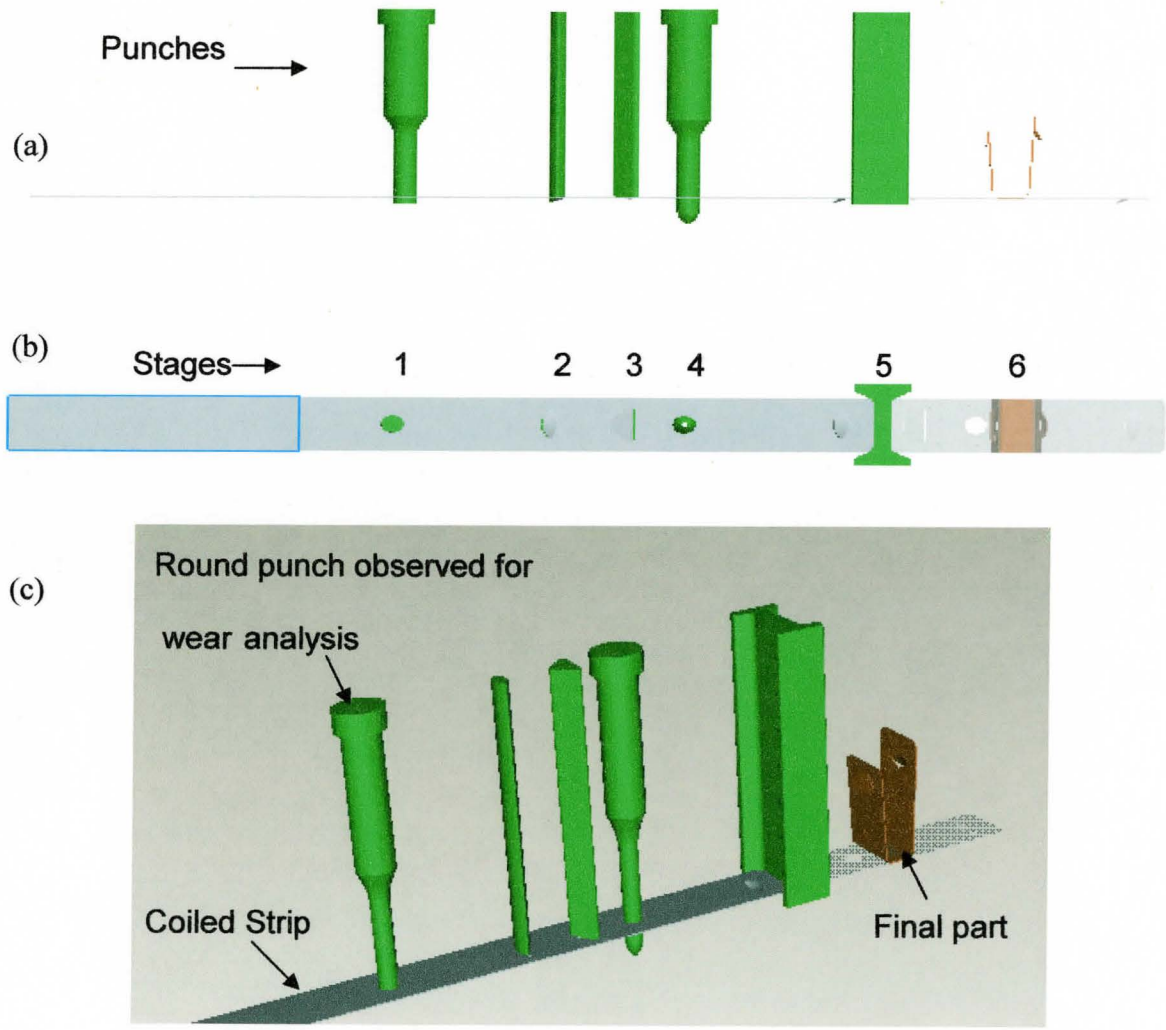

Figure 4-3 Strip layout (a) Front view (b) Plan (c) Isometric view.

Die Stage Number	Operation performed
1	Piercing
2	Lancing
3	Lancing
4	Piloting
5	Notching/parting
6	U - Bending

Table 4-3 Strip layout – list of stages.

4.3.2 Punch Details

The punches and die inserts were procured from a standard tooling supplier. The tool characteristics and material composition were obtained from EXACTA and are given in Tables 4-4 and 4-5.

Material	Hardness (HV)	Piercing Diameter(mm)
AISI M2	700	$\phi 5 \pm 0.03$

Table 4-4 Punch characteristics.

Material grade	Chemical composition						
	% C	% Si	% Mn	% Cr	% Mo	% W	% V
AISI M2	0.85	0.35	0.3	4.2	5.1	6.3	2

Table 4-5 Punch material composition (wt %).

A set of punches are coated with MoS_2 as shown in Table 4-6, at ION BOND Inc [www.ionbond.com] to study the wear behavior.

Coating type	Coating Thickness	Coating Hardness
MoS_2	3~5 micrometers	2000 HV

Table 4-6 Details of surface coating on punches [www.ionbond.com].

4.3.3 Determination of Normalized Abrasive Wear Rate (K')

To find out normalized abrasive wear rate, the weights of the punches were measured before and after the experiments and are given in the Table 4-7. Equation (3-17) was used to calculate normalized abrasive wear rate. An accurate digital balance available at McMaster (SARTORIUS), with 0.00001 g resolution was used to measure the weight of the punches. The calculated normalized abrasive wear rate was found to be very close to the value derived by L.Bourithis, 2005. The calculated values, shown in Table 4-7, were used in the proposed tool life models. The density of M2 tool steel material was taken as 7.8 g/cc.

	Punch size	Weight (in 'gms') Before	After	Force (in 'N')	No of strokes	Punch travel	K' (mm^3/Nmm)
Test-1	ϕ4.998	31.68456	31.66162	2.8675	47000	10	1.53776 E-09

Table 4-7 Calculation of normalized wear rate (K').

4.3.4 Normalized Adhesive Wear Rate (K'')

Previous studies [Bourithis, 2005] have found that the normalized wear rate due to adhesion (K'') is less than abrasive wear under the same conditions. In the present study, it was assumed as:

$$K'' = \frac{1}{3} K' \tag{4-1}$$

4.4 Test Matrix

The experiments were conducted using the above discussed U-clip progressive die. The test matrix is listed in Table 4-8.

	Punch size	Die size	Clearance (%)	Punch edge Radius (mm)
Test-1	ϕ4.998	ϕ5.080	10%	0.025
Test-2	ϕ5.000	ϕ5.080	10%	0.025
Test-3	ϕ4.998	ϕ5.080	10%	0.025
Test-4	ϕ4.969	ϕ5.080	17.5%	0.050
Test-5	ϕ 5.005 (Coated)	ϕ5.080	10%	0.025

Table 4-8 Test matrix.

Three samples of each part and round slug were collected after every 10,000 punching strokes. The parts were cleaned with acetone and stored in separate small plastic boxes.

4.5 Measurement Methods

4.5.1 Parameters Measured

The following parameters listed in Table 4-9 were measured on each sample from every test.

Item	Parameter measured	Device used
U-clip(part)	Hole size	Mitutoyo - CNC Quick Vision Zygo - Optical profiler
Round slug	Burr height	Mitutoyo - CNC Quick Vision Zygo - Optical profiler
Round Punch	Punch diameter	ZEISS - CMM

Table 4-9 Parameters measured and devices used.

4.5.2 Device Used for Burr Height Measurement

The importance of burr height measurement was discussed in section 2-5. The accuracy of the experimental results is dependent on the accuracy of

measurement; hence a suitable measuring device has to be selected. Mostly, conventional and optical measurements were used for burr height in the studies discussed in the section-2. In the present study, following two different devices were examined and finally the best one was selected.

4.5.2.1 ZYGO Optical Profiler

The ZYGO optical profiler (Figure 4-4), available at MMRI, is a powerful tool for characterizing and quantifying surface roughness, step heights, critical dimensions, and other topographical features with excellent precision and accuracy. All measurements are nondestructive, fast, and require no sample preparation. ZYGO delivers 0.1 nanometers height resolutions, for a range of surface texture, magnification, or feature height, all in a single scan.

Figure 4-5 shows the result of round slug burr height measurement using ZYGO. The scanning was done across the burr on the round slug to find out burr height. The 3D graph shows that the scanning could not pick up the burr properly due to sharp features of burr. Hence the ZYGO device is not the right device to measure burr height.

Figure 4-4 ZYGO optical profiler.

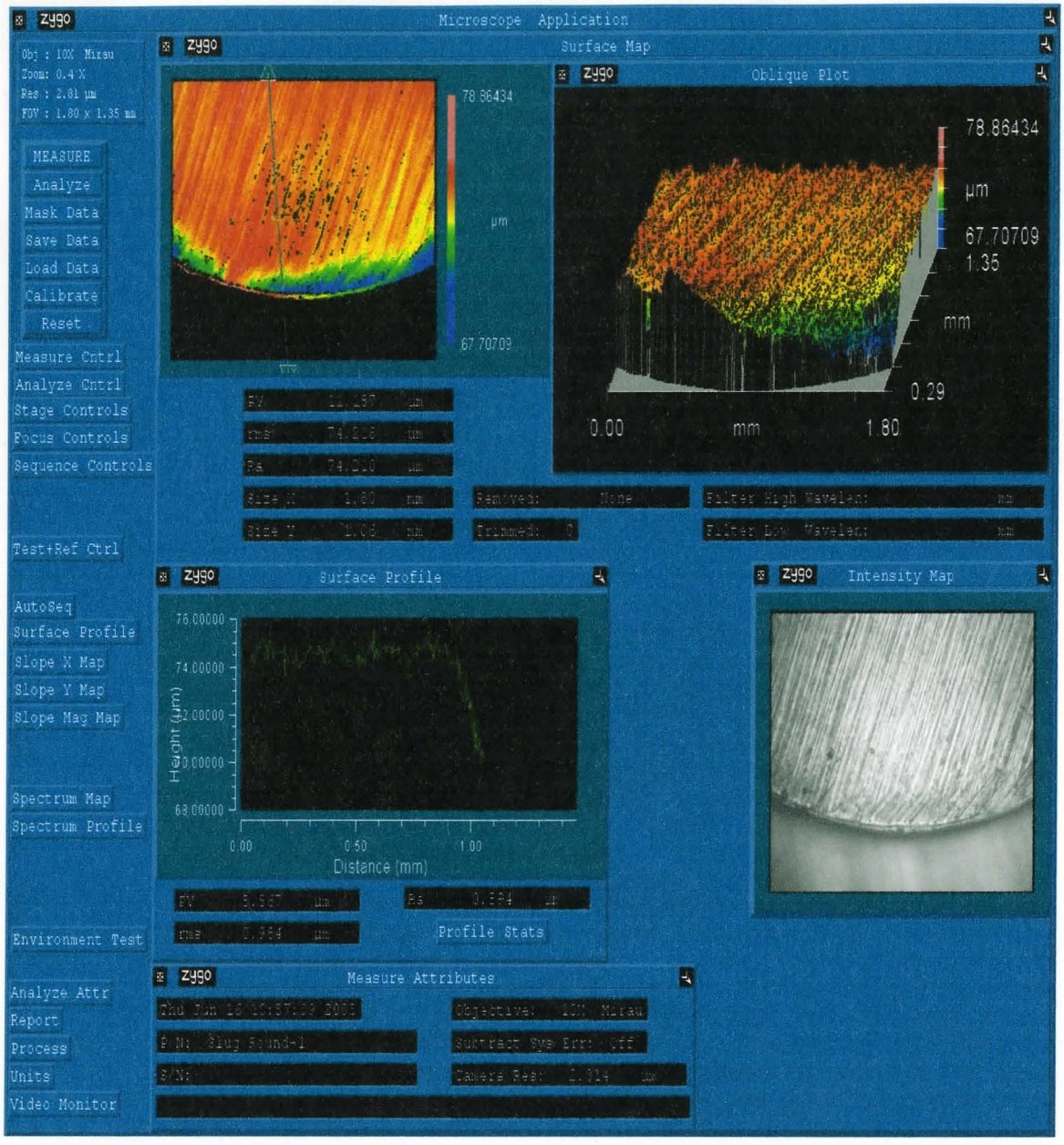

Figure 4-5 Burr height measurement using ZYGO.

4.5.2.2 Mitutoyo CNC Quick Vision System – ELF 200

The CNC quick vision system as shown in Figure 4-6, is an optical measuring device with crystallized glass scale with a resolution of 0.02 micrometers. The device can be used to measure step heights, critical dimensions, and other topographical features with excellent precision and accuracy. Like ZYGO optical profiler, all measurements are nondestructive, fast, and require no sample preparation.

The optical scan generates a view as shown in Figure 4-7. The height measurements were carried out by clicking the mouse on a desired burr surface on the image. The CNC system focuses on selected point and calculates the highest point from the reference plane. A large number of points were measured and the highest value was selected as the maximum burr height.

The CNC quick vision system turned out to be a better measuring device for burr height. The hole diameter of the U-clip was also measured using this device. The results are discussed in the next section

Figure 4-6 Mitutoyo CNC quick vision system.

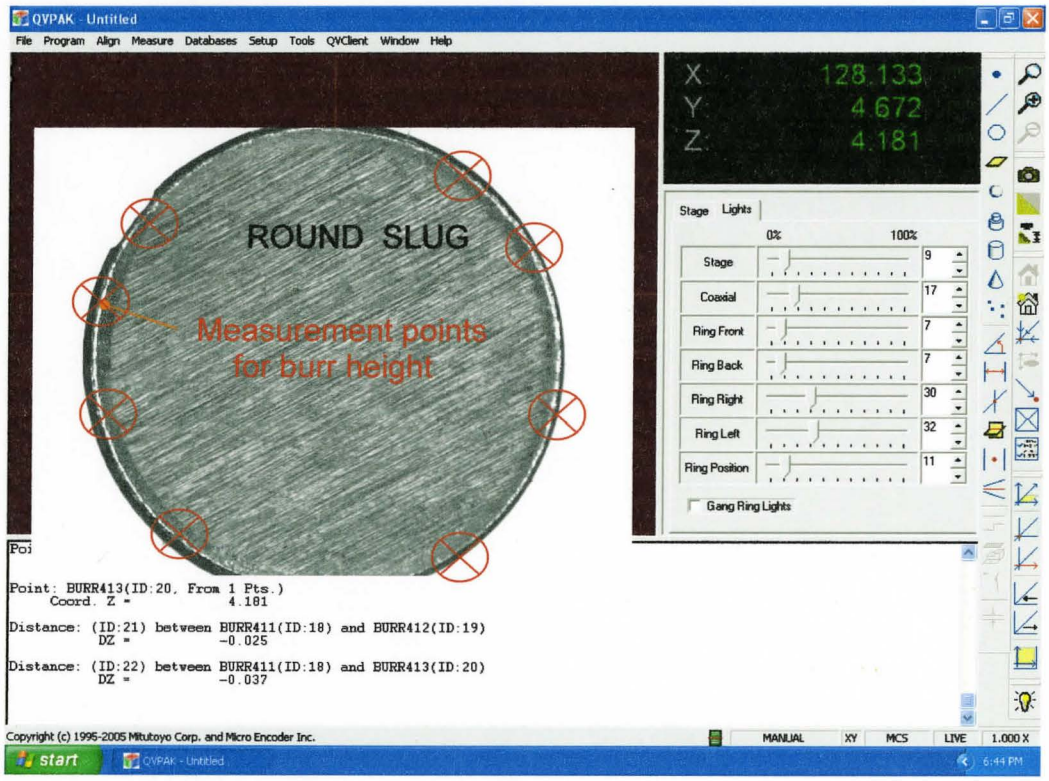

Figure 4-7 Measurement screen of Mitutoyo CNC quick vision system- Image of slug and burr height measurement points.

4.6 Experimental Results

4.6.1 Punch Wear

The punch diameter was measured before (D) and after (D_N) the test as listed in Table 4-10. The difference in punch diameters ($D - D_N$) was utilized to obtain punch wear. The image of the worn punch with flank and edge wear is shown in Figure 4-8. The SEM images were taken before punching as shown in Figure 4-9 and show the sharp punch edge. The punch edges became dull during punching due to wear as shown in Figure 4-10.

	Initial punch diameter D ('mm')	Number of Punching Strokes N	Final punch diameter D_N ('mm')	Diametrical Wear $D - D_N$ ('mm')
Test 1	ϕ4.998	100,000	ϕ4.951	0.047
Test 2	ϕ5.000	43,000	ϕ4.980	0.020
Test 3	ϕ4.998	60,280	ϕ4.971	0.027
Test 4	ϕ4.969	42,725	ϕ4.949	0.020
Test 5	ϕ5.004 (Coated)	10,000	ϕ5.000	0.005

Table 4-10 Punch wear results.

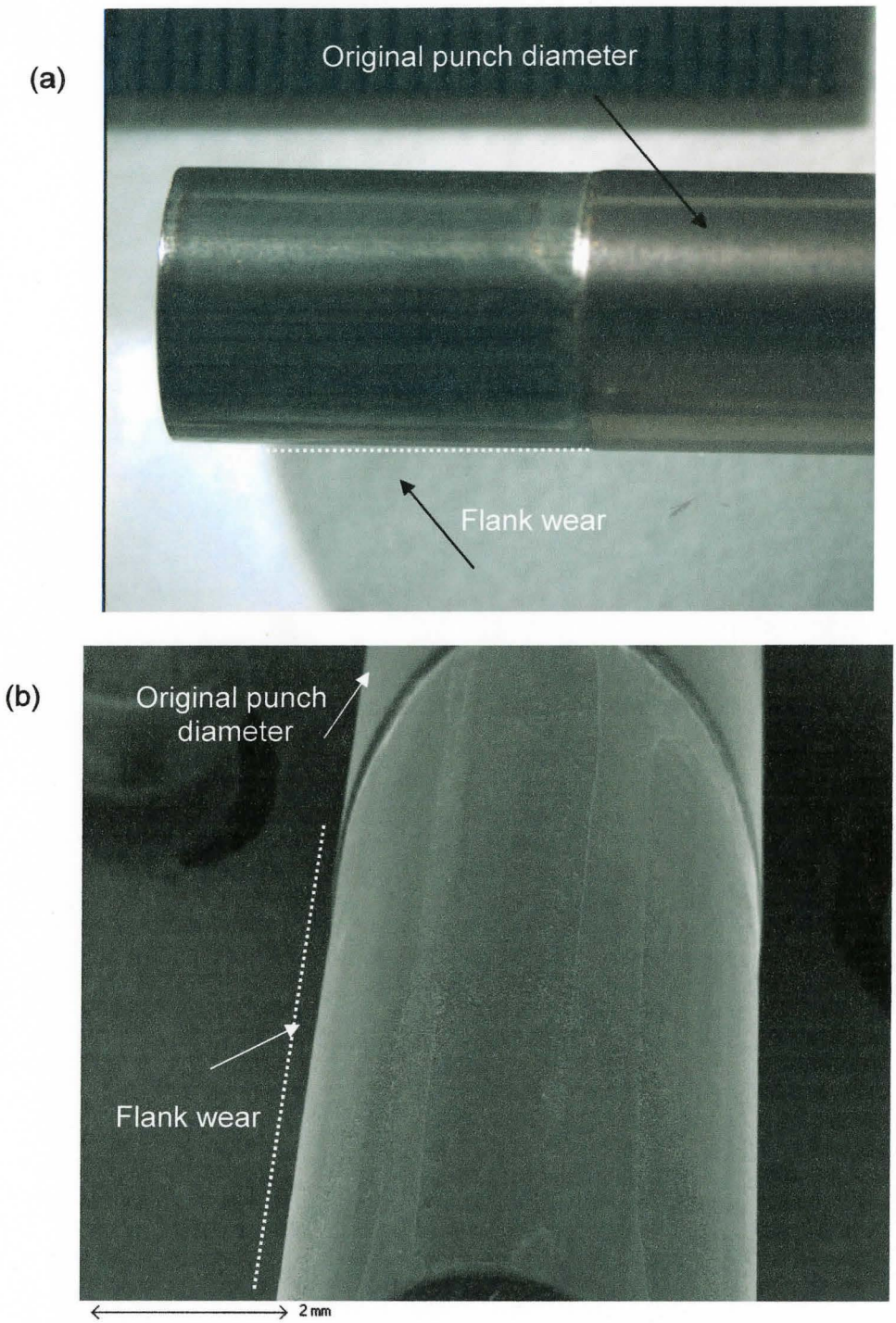

Figure 4-8 Images of a worn punch with flank wear
(a) Microscope image (5X) and (b) SEM image (7X).

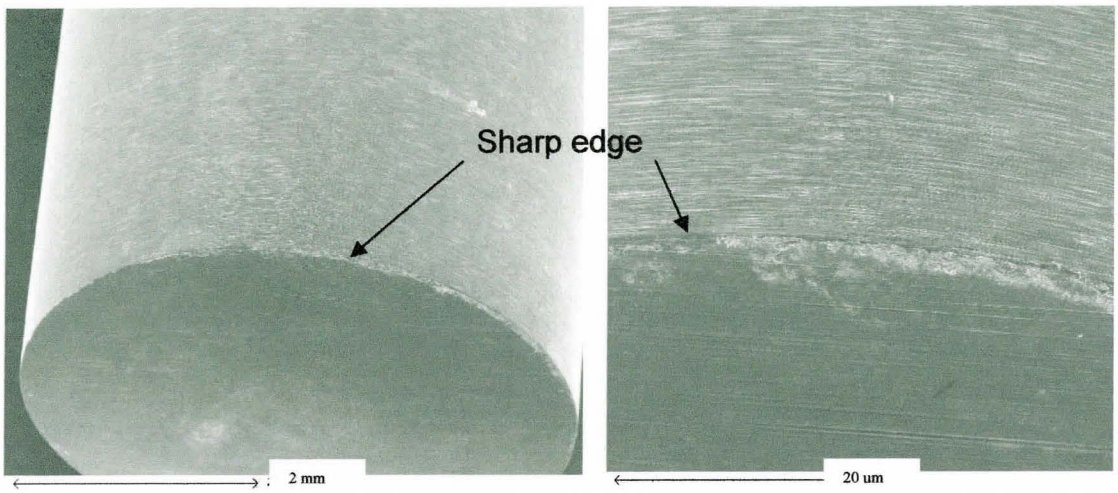

Figure 4-9 SEM images of punch edge before punching.

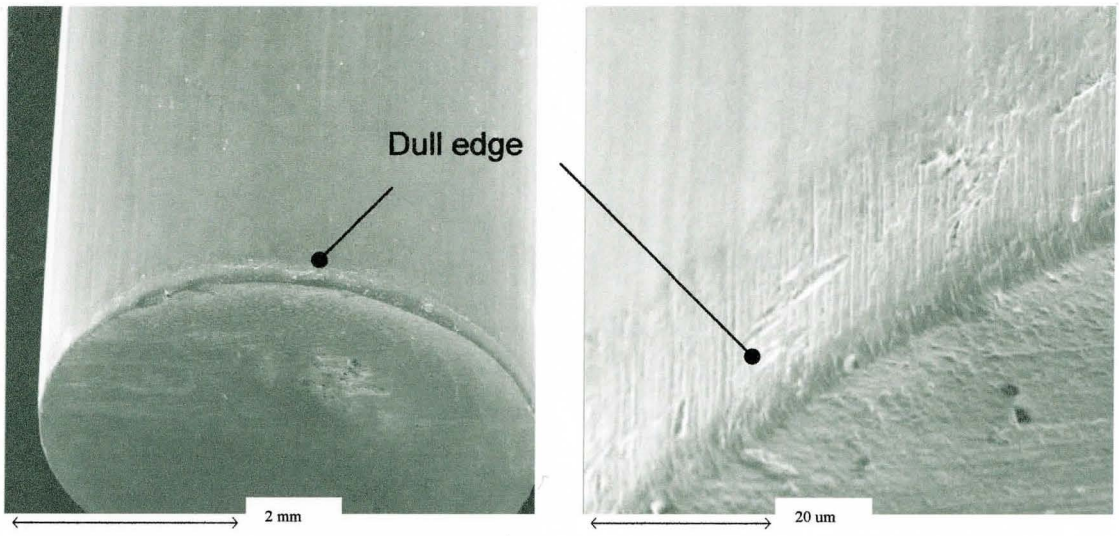

Figure 4-10 SEM images (10X) of punch edge after 100,000 punching.

4.6.2 Burr Height (b)

Burr height on the round slug was measured using Mitutoyo CNC vision system as discussed in the section 4.5.2.2 and the summary of results are listed in Table 4-11 (Details are listed in Appendix B). The images of slugs after various punching strokes are shown in Figure 4-11 and 4-12. It is clear from the results and images that the burr height (b) is increased gradually with the number of punching strokes (N).

Test 1	1	2	3	4	5	6	7	8	9	10
N *(in'000')*	5.4	12	19	27	37	53	59	76	85	100
b *(in 'μm')*	75	79	83	90	96	108	116	121	127	138

(a)

Test 4	1	2	3	4	5	6	7
N *(in'000')*	0	4.7	12.2	20	26.3	32	42.8
b *(in 'μm')*	97	108	119	122	124	136	142

(b)

Table 4-11 Burr height measurements- experimental results of (a) Test 1 and (b) Test 4.

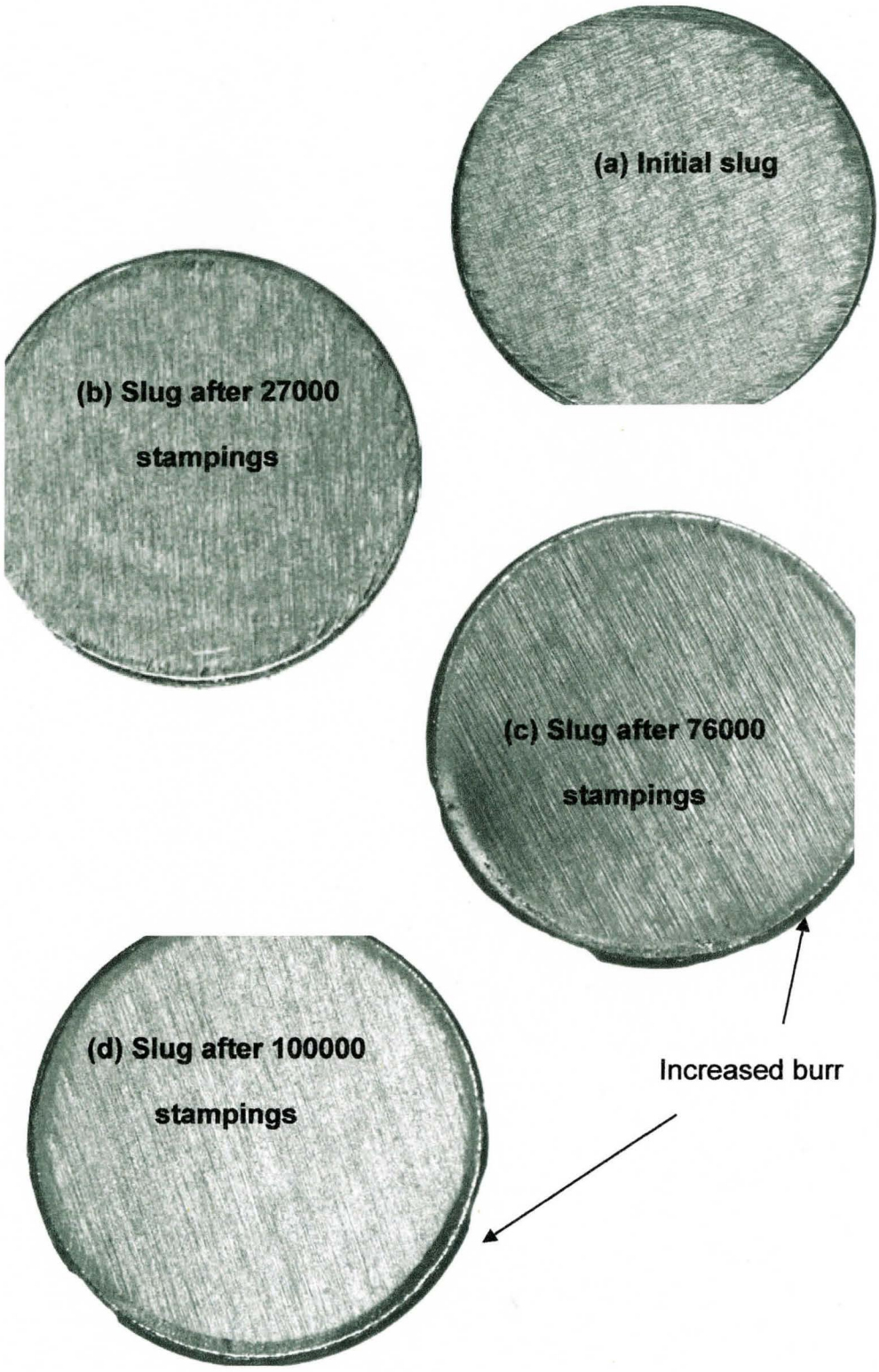

Figure 4-11 Slug images (10X) after different number of punching.

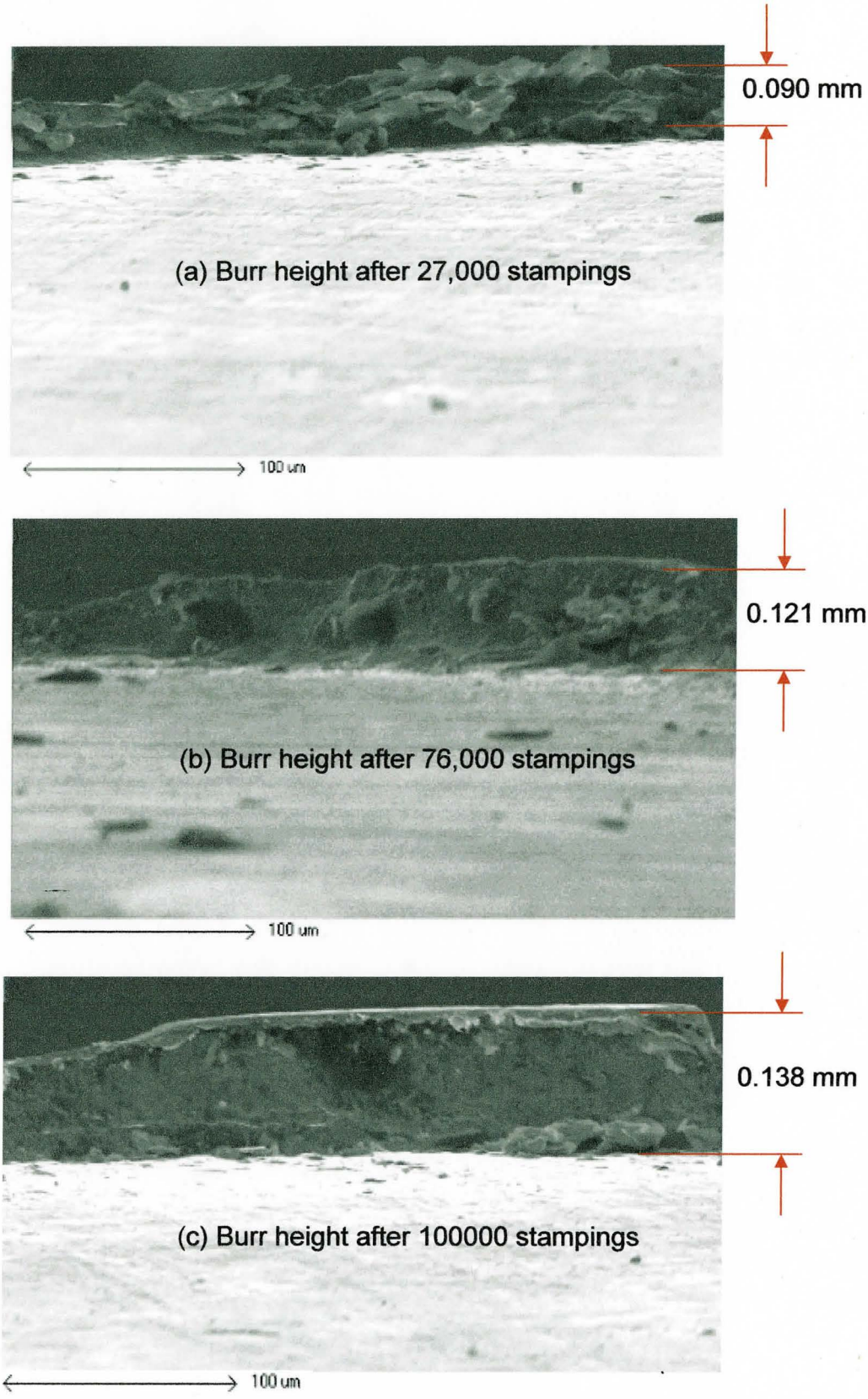

Figure 4-12 SEM images of burr (300X) after different number of punching operations.

4.6.3 Pierced Hole Diameter (D_N)

Hole size on the U-clip was measured using Mitutoyo CNC vision system and the summary of results are listed in Table 4-12 (Details are listed in Appendix B). It is clear from the results that the hole size is decreased gradually with the number of punching strokes (N).

Test 2	1	2	3	4	5	6	7	8
N *(in'000')*	0	4.2	10	20	26.8	34.5	40	43
D_N *(in 'mm')*	ϕ4.996	ϕ4.994	ϕ4.990	ϕ4.987	ϕ4.984	ϕ4.98	ϕ4.978	ϕ4.977

Test 4	1	2	3	4	5	6	7
N *(in'000')*	0	4.7	12	20	26.3	32	42.8
D_N *(in 'mm')*	ϕ4.959	ϕ4.957	ϕ4.952	ϕ4.95	ϕ4.948	ϕ4.942	ϕ4.939

Table 4-12 Hole size results.

(a)

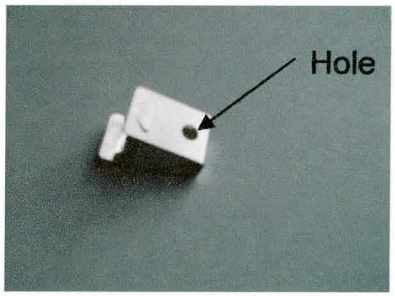

(b)

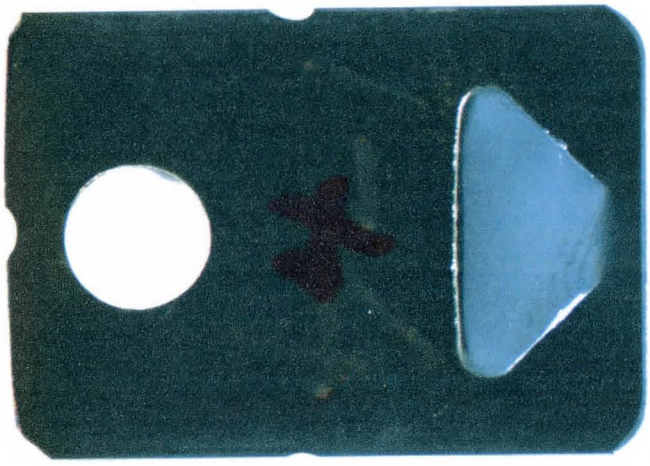

Figure 4-13 U-Clip with hole (a) whole part
(b) partial part prepared for measurements.

4.7 Summary of Experiments and Results

The objective of conducting experiments as discussed in the present Chapter 4 is to validate the new analytical tool life model proposed in the present study (Chapter 3). The measurement technique used in the present study is a novel attempt to obtain accurate results when compared to previous works discussed in the Chapter 2. The experimental results of burr height and wear are compared with the analytical model in Chapter 6. In addition to experimental work, an attempt is made to compare the new tool life model with a FE model, which is presented next in Chapter 5.

Chapter 5

FE Modeling of Hole Piercing

In the last few years, simulation methods based on finite element analysis have lead to a better understanding of the metal forming process and can improve product and tool design. The aim of FE modeling in the present study is to understand the influence of punch edge radius and clearance on burr height and to compare the results with the proposed model and experiments discussed in chapters 3 and 4 respectively.

Finite element method is generally composed of three basic steps, namely: preprocessing of input data, computational analysis, and post-processing of data to obtain relevant results. The input data includes the blank geometry, development of a suitable mesh for the blank, selection of a yield criterion and hardening law, definition of the contact, boundary conditions, applied loading and incorporation of a strain based criterion for fracture for models involving material separation. Computational analysis involves solving a large set of equations arising from assembling a large stiffness matrix of the deformed body (blank). The solution of equations provides displacement field and thus the deformed shape of the blank at various stages of piercing process. The

displacement along with stress and strain in the part can be visualized or extracted during post-processing. Post processing is a final step to obtain results from simulation runs and provide predicted shapes as well as stress strain data. In this chapter, details of all the three steps of FE modeling are presented.

5.1 Input Data

5.1.1 Analysis Type

5.1.1.1 Implicit versus Explicit

Implicit and explicit analyses are capable of solving a wide variety of problems. The characteristics of implicit and explicit procedures determine which method is appropriate for a given problem. Implicit analysis solves for equilibrium at the every time step $(t + \Delta t)$ whereas, explicit method solves for equilibrium at time t by direct time integration. Implicit method but may have difficulty converging because of contact or material complexities, resulting in a large number of iterations. Such analyses are expensive because each iteration requires a large set of linear equations to be solved. Explicit method determines the solution without iterating by explicitly advancing the kinematic state from the previous increment. Another advantage of explicit method is that it requires less computer disk space and memory than implicit method for the same simulation.

In the present study of hole piercing, ABAQUS/Explicit FE code along with "Explicit Dynamic", analysis was used in the rate independent plasticity model. A brief description of this method is discussed in the next section.

5.1.1.2 Explicit Dynamic Finite Element Method

A nonlinear structural problem is one in which the structure's stiffness changes as it deforms. All physical structures are nonlinear. Linear analysis is a convenient approximation that is often adequate for design purposes. It is obviously inadequate for many structural simulations including manufacturing processes, such as forging or stamping; and analyses of rubber components, such as tires or engine mounts.

The explicit dynamics method was originally developed to analyze high-speed dynamic events that can be extremely costly to analyze using implicit programs. As an example of such simulation, the effect of a short-duration blast load on a steel plate can be analyzed. Since the load is applied rapidly and is very severe, the response of the structure changes rapidly. Accurate tracking of stress waves through the plate is important for capturing the dynamic response. Since stress waves are associated with the highest frequencies of the system, obtaining an accurate solution requires many small time increments.

At the beginning of the increment the program solves for dynamic equilibrium, which states that the nodal mass matrix, M, times the nodal accelerations, $\ddot{u}$, equals the total nodal forces (the difference between the external applied forces, P, and internal element forces, I):

$$M\ddot{u} = P - I \tag{5-1}$$

The summary of the explicit dynamics algorithm is given in the Figure 5-1.

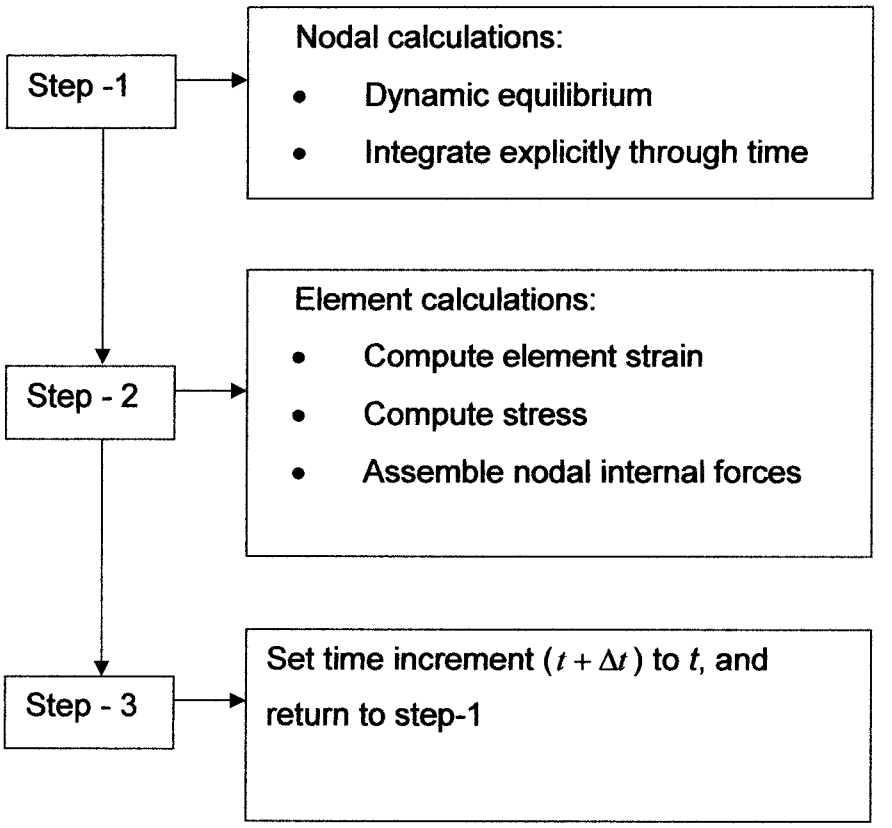

Figure 5-1 Explicit dynamic algorithm.

5.1.2 Geometry Modeling

Hole piercing process was treated as a 2D or plane strain process in the modeling. The punch, die and stripper were represented as rigid materials. The model geometry is shown in Figure 5-2. In ABAQUS, each of the tools can be represented as analytical rigid surfaces. Each of the rigid surfaces is associated with a reference node (RF) on which boundary conditions specifying tool motion and constraints are applied.

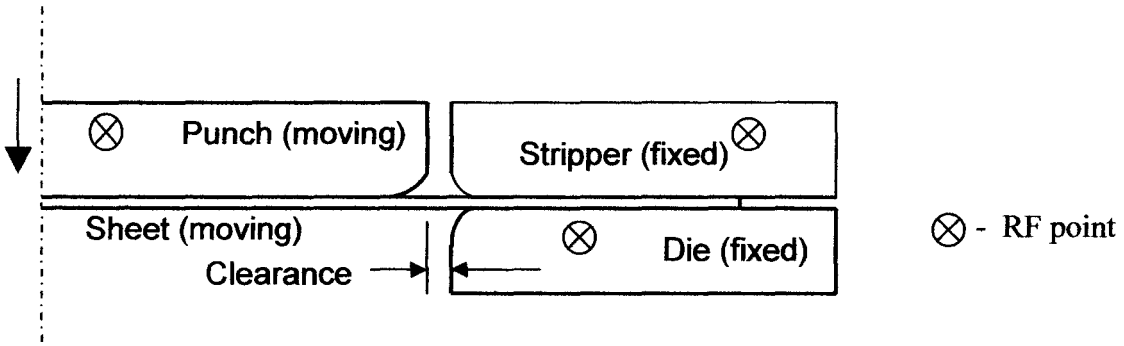

Figure 5-2 Model Geometry.

5.1.3 Material Modeling

The material behavior is represented in terms of elastic (Young's modulus and poisons ratio) and plastic properties in terms of stress-strain data. These material properties in FE analysis are needed to construct the constitutive matrix.

The material is considered as elastic, isotropic and rate independent. The effect of anisotropy is neglected in the analysis. The various material parameters used as input to the model are presented in Table 5-1.

Property	Sheet	Tooling
Material	AISI 301	Steel
Density (Kg/m^3)	7800	
Young's Modulus (GPa)	193 GPa	200 GPa
Poisson's ratio	0.33	0.33
Yield Stress (MPa)	1300	-----
Coulomb's friction coefficient	0.3	

Table 5-1 Material definition in ABAQUS.

5.1.4 Tool-Sheet Contact

Contact problem is perhaps one of the most critical in the modeling of hole piercing process because it concerns many issues including surface property definition for the tools and new contact generation as the tools come in contact with the blank. A "contact pair" is defined in ABAQUS to establish the contact between deformable blank and rigid tools. For hole piercing, three contact pairs are possible as shown in Figure 5-3.

A contact pair consists of a master surface, normally a rigid surface and a deformable slave surface. Definition is mainly based on the strength or hardness of the material. In general, master surface has a higher strength (Young's modulus) compared to the slave surface.

The contact and sliding between the master and slave surfaces is mainly controlled by friction, since there is always normal pressure from a master surface, and a relative movement between a contact pair. Due to the complexity and limited study on this subject, in current model, only a constant frictional coefficient was considered.

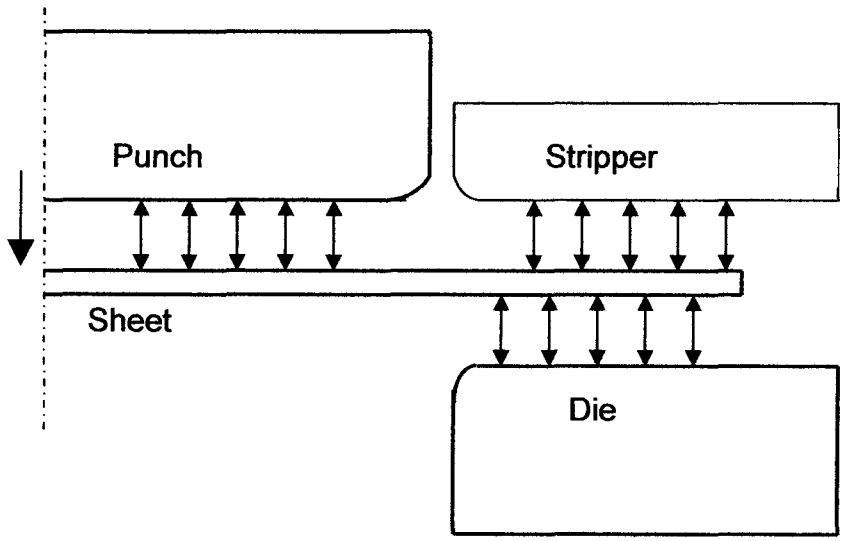

Figure 5-3 Contacts of tooling and sheet.

5.1.5 Boundary Conditions and Loading

Two types of boundary conditions were used in modeling. "Displacement" option was set to die and stripper, which were fixed in all directions. "Velocity" option was set to punch and defined as constant in "y" direction, but was restricted in "x" direction. Rotation of the punch was also fixed. Sheet was free to move in both directions. The boundary conditions were shown earlier in Figure 5-2 and 5-3.

5.1.6 Meshing

A fracture criterion was implemented in the FE model to simulate the material separation process. For this purpose, the sheet was partitioned into three zones as shown in Figure 5-4. In central area, a fine mesh of 50 x 50 elements and a coarse mesh in the slightly deformed (and therefore less important) regions of the blank was used. Since quadrilateral (4-noded) element gives better accuracy than the triangular element, CPE4R (a quadrilateral plane strain element in ABAQUS) was used in the present study.

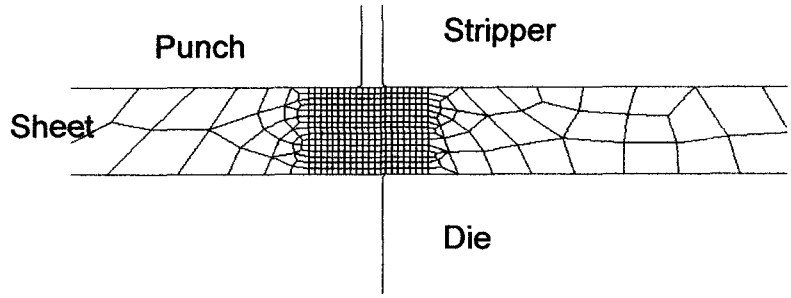

Figure 5-4 A sketch illustrating partition in the mesh used.

5.1.7 Fracture Criterion and Element Deletion Method

Two popular methods often used in FEM software to handle material failures are: nodal separation and element deletion. Taupin [Taupin, 1996] proposed "element deletion" technique. Element deletion method is good choice since it is easier to handle. Damaged element was removed when a critical value of damaged parameter was reached as shown in Figure 5-5. This mechanism provided a promising approach to approximate the shape of cut edge.

However, element deletion approach has some shortcomings. Firstly, an element deletion does not have any physical meaning because of a loss in mass continuity. Secondly, the shape of the cut edge and accuracy of load calculation

are largely influenced by mesh size. Thirdly, element deletion does not stand for crack propagation; removal of elements using the element deletion methodology modifies the effect of the crack tip. But, not all these disadvantages are formidable. A mass loss and mesh size should not be a problem. If a fine mesh is utilized. Deleted elements constitute just a small portion. A large number of element and a fine mesh are now viable due to increased computational efficiency of recent years. Insufficient representation of crack propagation still remains to be a problem.

ABAQUS/Explicit can handle element deletion and was used in the present work. For a shear failure, the following syntax was used in ABAQUS/Explicit.

Shear failure = γ_t, element deletion = yes

In the present work, the fracture strain was obtained from numerical prediction proposed by Atkins et al. (equation 2-6). The same value was also used in the proposed new analytical tool wear/life model in the present work. ABAQUS/Explicit input code for hole piercing simulation is presented in Appendix C for test matrix-1. Results of simulations are presented in the next section and compared with the new analytical tool life model and experiments in chapter 6.

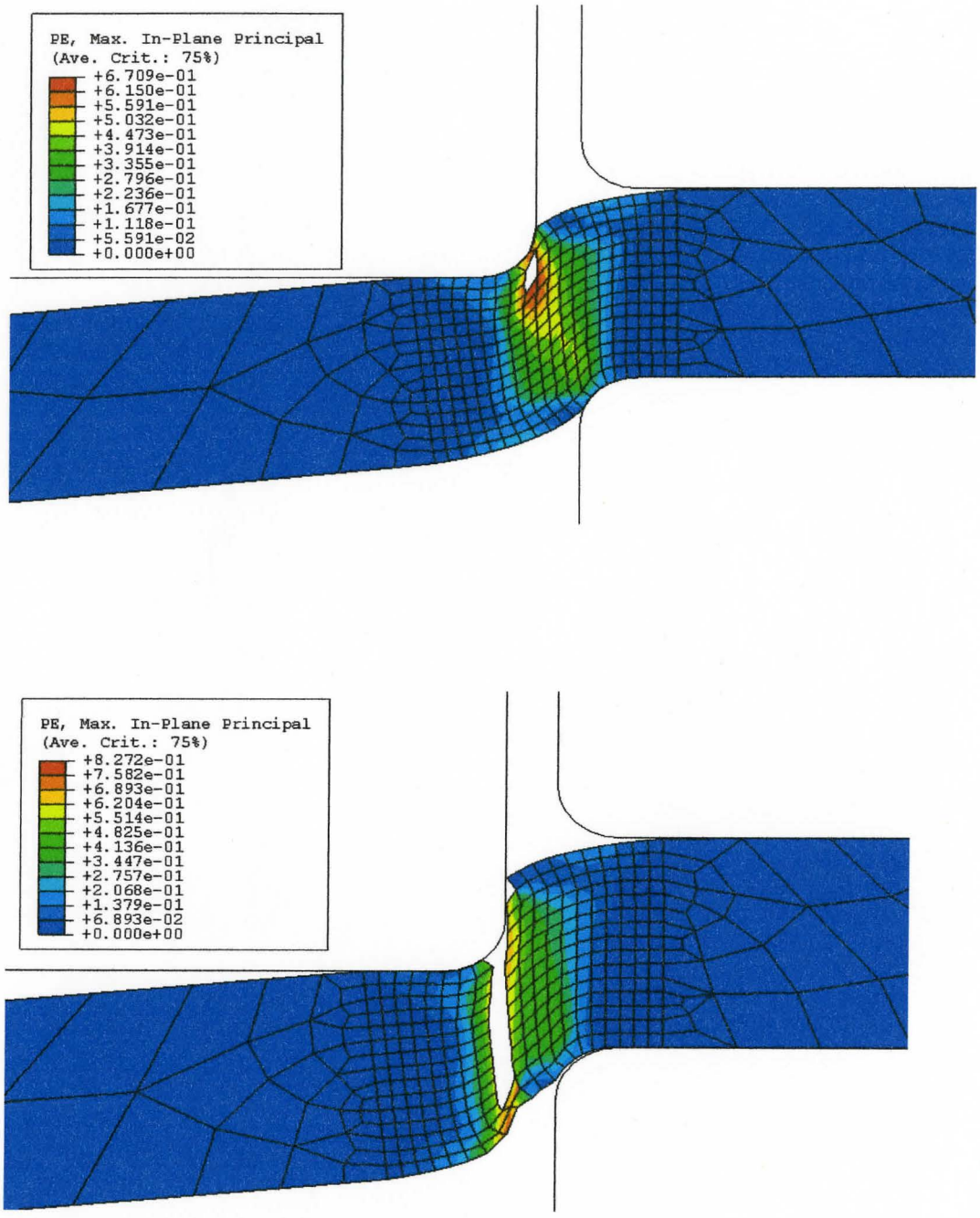

Figure 5-5 A sketch illustrating element deletion method in ABAQUS (a) beginning and (b) end of element deletion process.

5.1.8 Tool Set Configuration

Simulations with four different tool configurations (Table 5-2), same as in the experiments, were carried out. The results are given in the next section. The burr size from the simulations is compared with the new tool life model and experiments in the Chapter 6.

Simulation	Punch size (mm)	Die size (mm)	Clearance (%)	Punch/die edge radius (mm)
1	ϕ4.998	ϕ5.080	10%	0.025
2				0.100
3	ϕ4.969	ϕ5.080	17.5%	0.050
4				0.110

Table 5-2 Tool set configuration for FE simulations

5.2 FE Simulations and Results

5.2.1 Simulation of Hole Piercing

An advantage of FE analysis lies in its ability to provide a snap shot of the deformation process and the material flow pattern through the thickness that can not be captured in experiment. Simulation results in the form of punch load

versus punch displacements were extracted from FE simulations for tool set configuration-1 and are shown in Figure 5-6.

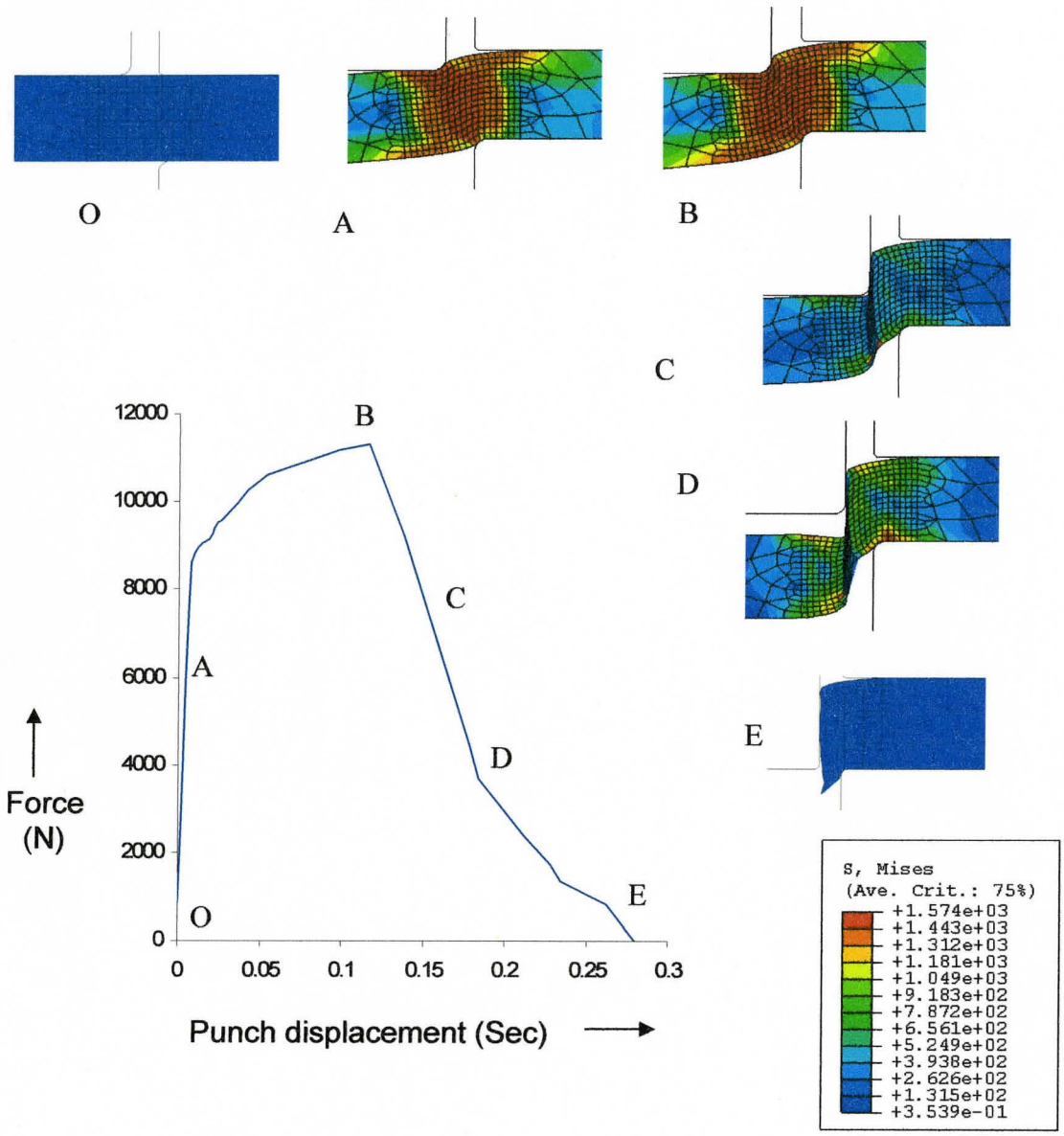

Figure 5-6 Typical stages of hole piercing process in FE simulation.

The progress of hole piercing process during the simulation is shown as images depicting rollover, sheet indentation, fracture initiation, propagation through thickness and hole formation. The presentation is similar to the earlier discussion presented in the Section 2-1 of Chapter 2 (Literature review). The results of simulations shown in Figure 5-6, follow the same sequence (stages from O to E) as in the Figure 2-1, discussed in the literature review. The colour matrix in the sheet represents various stress levels as per the scale shown in Figure 5-6. The red colour zone represents higher level of stress which was dominant during sheet indentation stages A to C; where as blue colour represents lower level stress which was dominant during sheet fracture initiation and propagation (stages from D to E).

5.2.2 Bending of Sheet

One of the important assumptions made in the new analytical model proposed in the chapter 3 was the sheet bending during piercing operation. The results from FE simulation confirms that the sheet was subjected to bending before punch penetration. The angle of bend was increased from 1° to 2° with the increase in clearance from 10% to 17.5% as shown in the Figure 5-7 which is in good agreement with the model proposed by Klingenberg et al.

Often, springback of sheet was noticed in piercing process due to the bending which in turn is responsible for the hole size variation after piercing. The effect of springback and amount of hole size variation is one of the important parameters in the present study and is discussed in detail in the next section. Figure 5-7 shows the strain contours for two different clearances values (10% and 17.5%). The stresses are more uniformly distributed in the clearance region for a clearance of 17.5%. Also, there is an increased bending of the material underneath the punch at the larger clearance

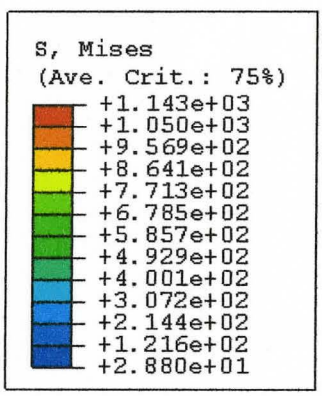

(a)

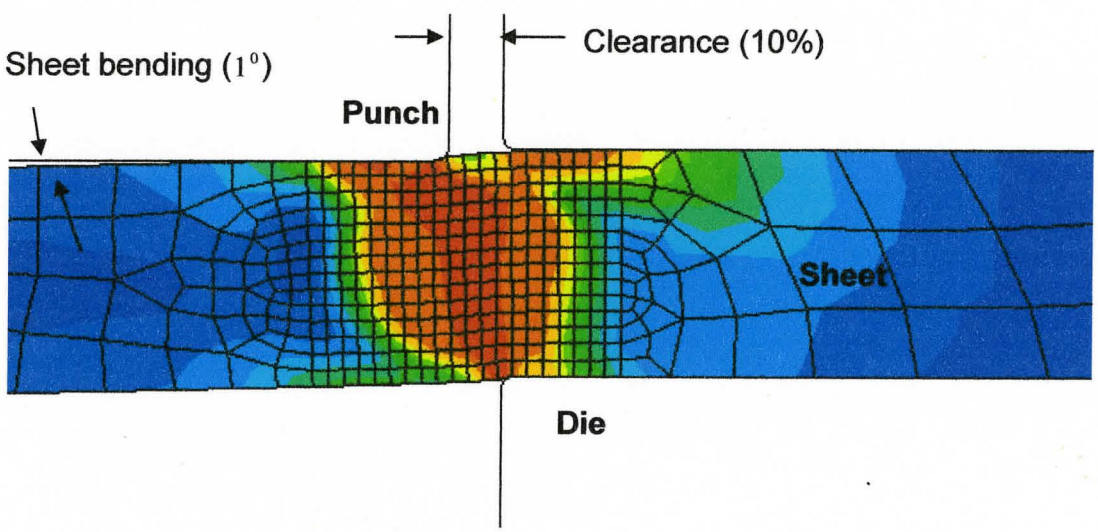

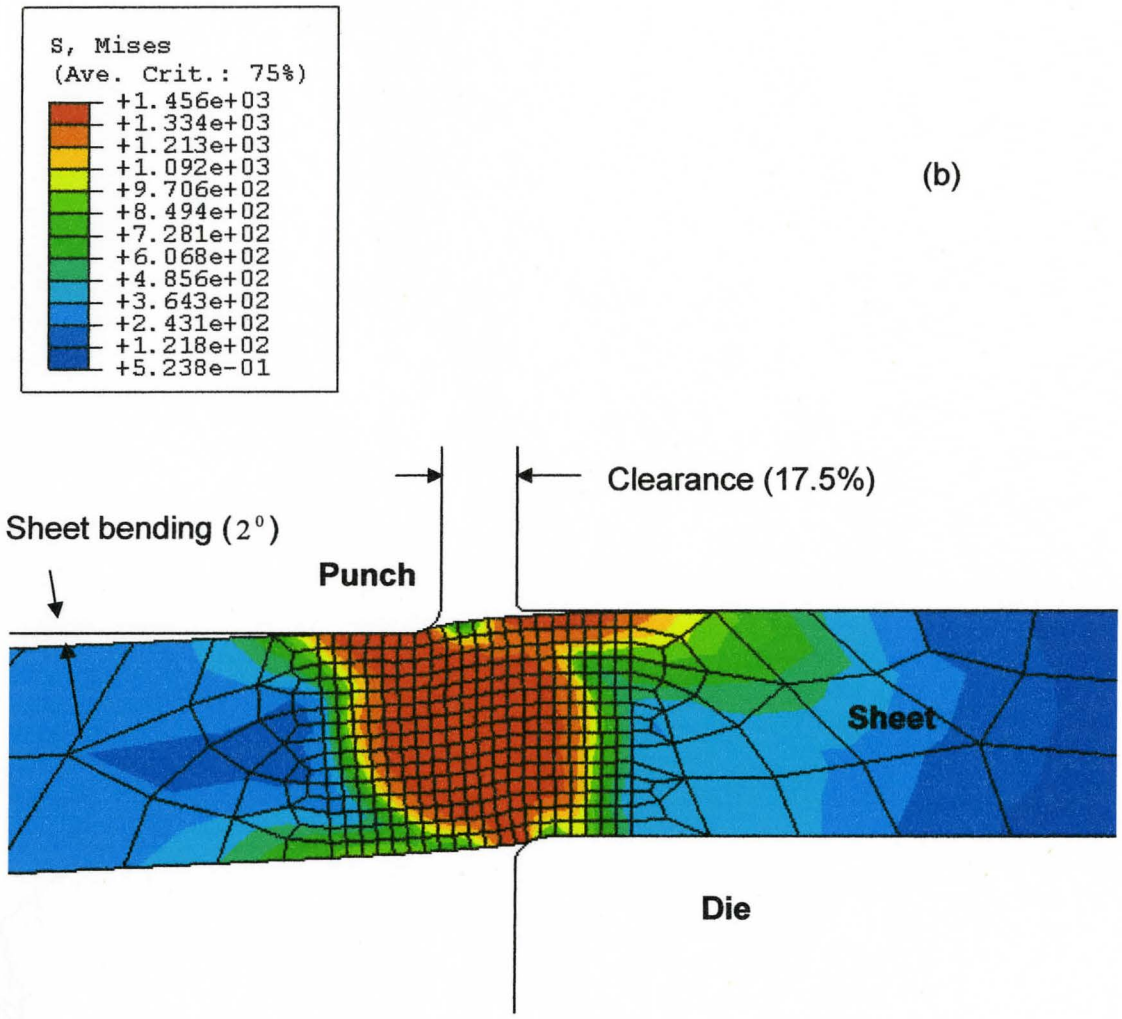

Figure 5-7 FE simulation showing bending of sheet with different punch/die clearance of (a) 10% and (b) 17.5% (at same punch displacement).

5.2.3 Burr height

Results from FE simulation have shown that burr height has increased with increase in clearance from 10 % to 17.5% as shown in Figure 5-8.

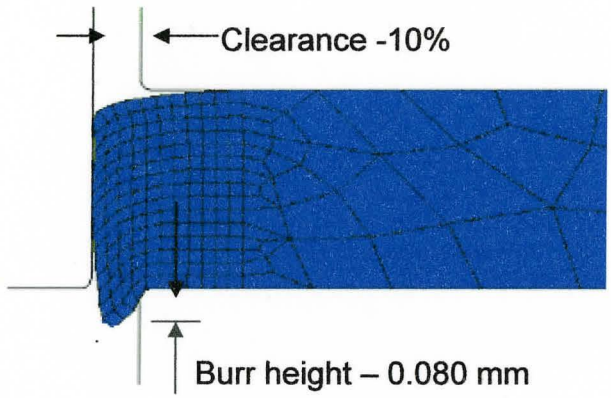

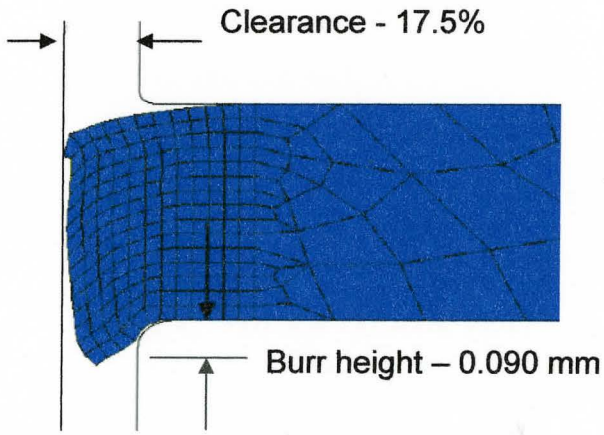

Figure 5-8 Burr height results from FE simulations.

5.2.4 Punch Force

FE simulations have shown that the change in maximum punch force was not significant with the change in clearance from 10% to 17.5%. But, the punch displacement has increased sharply for all the stages of piercing with the increase in clearance.

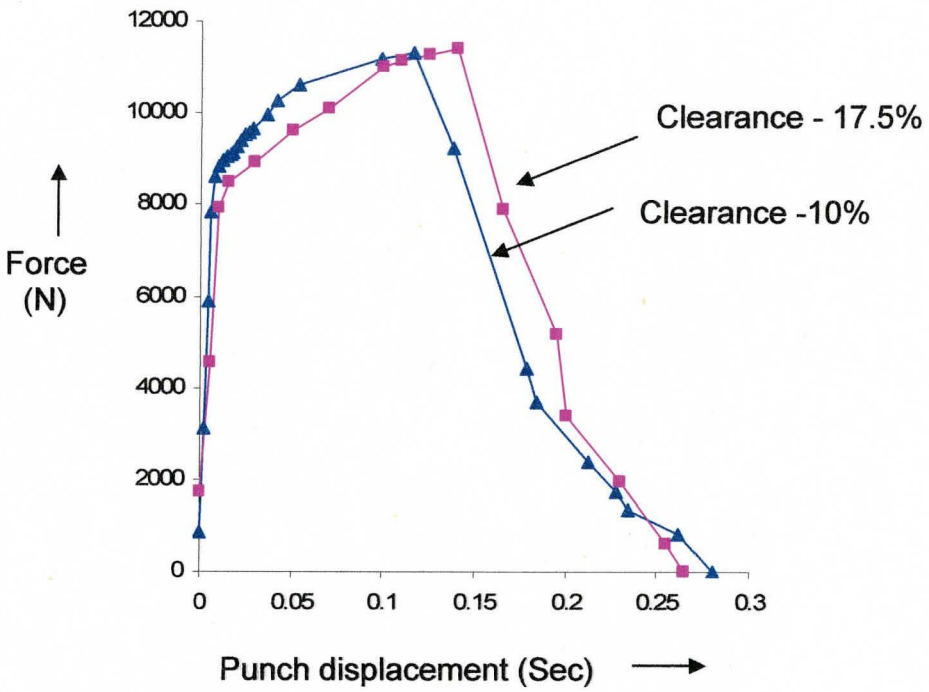

Figure 5-9 Blanking force comparison – results from FE simulation.

5.3 Summary of FEA Results

FE simulations using ABAQUS FE/Explicit code were studied to analyze hole piercing process with respect to sheet bending, punch penetration, punch force and burr formation. The parameters were simulated with two different tool set configurations having different clearances and punch/die edge radius. The results are compared and discussed in chapters 6 and 7 with reference to the new analytical model and experimental results.

Chapter 6

Model Predictions and Comparison with Experimental and FE Modeling Results

6.1 Punch Wear

The experimental results and theoretical predictions based on punch wear are given in Table 6-1. The punch used in Test-1 has produced about 100,000 parts from its beginning size of ϕ4.998 mm. The punch size at the end of punching after the test -1 was ϕ4.954 mm. The prediction from tool life model-1 is about 94,536 parts which is less by 5 % from experiment. The experiments were repeated with new punches on the same U-clip progressive die for the repeatability. The maximum and minimum difference between experiments and model prediction is about 8% and 5% respectively.

	Number of punching (N)		Difference
	Test	Model	(%)
Test 1	100,000	94,536	5
Test 2	43,000	39,501	8
Test 3	60,280	57,224	5
Test 4	42,725	39,500	8

Table 6-1 Punch wear - comparison of test and model predictions.

6.2 Burr Height

The results of burr height from model and experiments are shown in Table 6-2 and Figure 6-1. The clearance and punch edge radius in the model and experiment for Tests 1 and 4 were 10%, 17.5% and 0.025, 0.05 mm respectively. The experimental results and model predictions are in good agreement. The results show that burr height has linearly increased in the model as well as in the experiments with an increase in punch edge radius and clearance. The value of burr height was more in Test-4 than in Test 1 due to higher initial values of punch edge radius and clearance.

	Sample	Burr height (b)(in' μm ')		Difference (%)
		Test	Model	
Test 1	1	75	81	7
	2	79	91	13
	3	83	99	16
	4	90	106	15
	5	96	113	15
	6	108	124	13
	7	116	127	9
	8	121	136	11
	9	127	141	10
	10	138	147	6
Test 4	1	97	100	3
	2	108	118	8
	3	119	128	7
	4	122	137	11
	5	124	142	13
	6	136	147	7
	7	142	153	7

Table 6-2 Burr height – comparison of model with Test 1and 4.

(a)

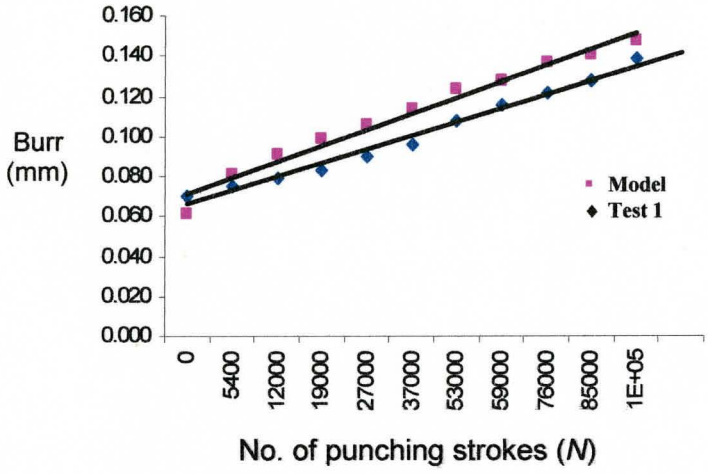

(b)

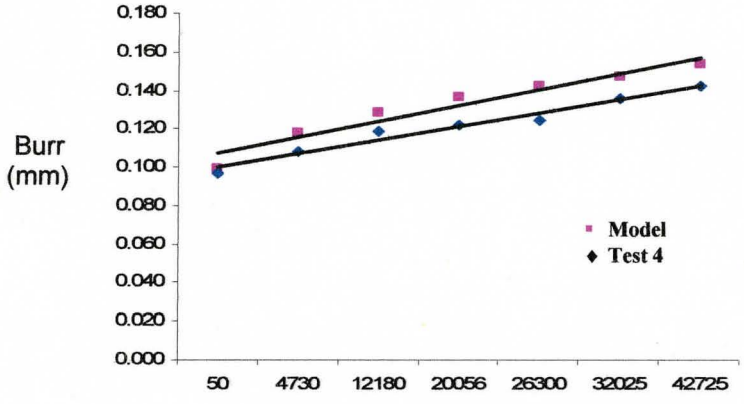

Figure 6-1 Burr height on slugs - comparison of (a) Test 1 and (b) Test 4 results with new tool life model predictions.

6.2.1 Comparison with Results from FE Simulations

The results from FE simulation on burr height were compared with the results from the new tool life model and experiment as shown in Table 6-3. The burr height was increased with increase in clearance in all cases. This shows that the new model is in good agreement with experiments and FE modeling.

	Sample	Clearance (%)	Edge radius (mm)	Burr height (b)(in μm)		
				Model	FEM	Experiment
Test 1	1	10%	0.025	81	80	75
Test 4	1	17.5%	0.050	100	92	97

Table 6-3 Burr height - comparison of new model with results from FE simulation and experiments.

6.3 Hole Size

The results of pierced hole size from model and experiments are shown in Table 6-4 and Figure 6-4. The results show that the hole size has decreased linearly in the model as well as in the experiments due to punch wear. However, the actual hole diameter was found to be less than the predicted value. The difference in hole size between model and Test 4 was more when compared to Test 2. The experimental results and model predictions are in good general agreement.

Sample	*Hole size (in mm)* Experiment	Model	Difference (%)
Test 2			
1	ϕ4.994	ϕ5.000	0.12
2	ϕ4.992	ϕ4.998	0.12
3	ϕ4.990	ϕ4.995	0.10
4	ϕ4.984	ϕ4.990	0.12
5	4.980	ϕ4.986	0.12
6	ϕ4.975	ϕ4.983	0.16
7	ϕ4.973	ϕ4.980	0.14
8	ϕ4.971	ϕ4.978	0.14
Test 4			
1	ϕ4.959	ϕ4.969	0.20
2	ϕ4.957	ϕ4.967	0.20
3	ϕ4.952	ϕ4.963	0.22
4	ϕ4.950	ϕ4.960	0.20
5	ϕ4.948	ϕ4.957	0.18
6	ϕ4.942	ϕ4.954	0.24
7	ϕ4.939	ϕ4.949	0.20

Table 6-4 Hole size – Comparison of tool life model with Test 2 and 4.

(a)

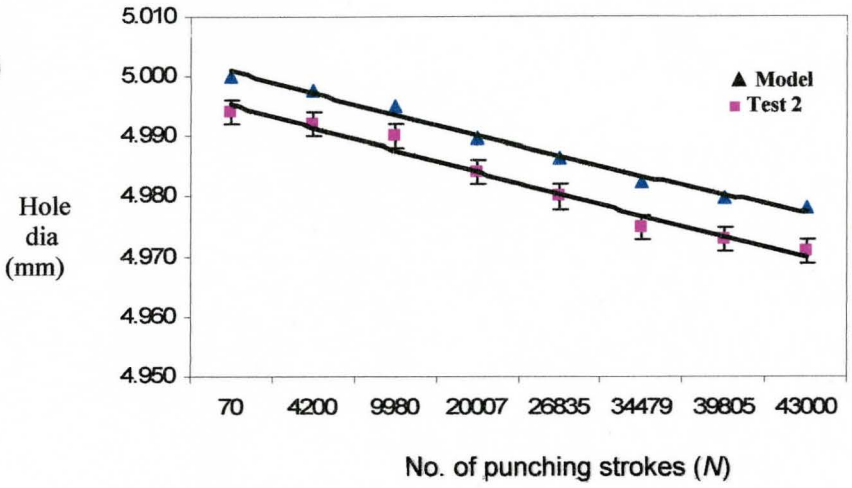

(b)

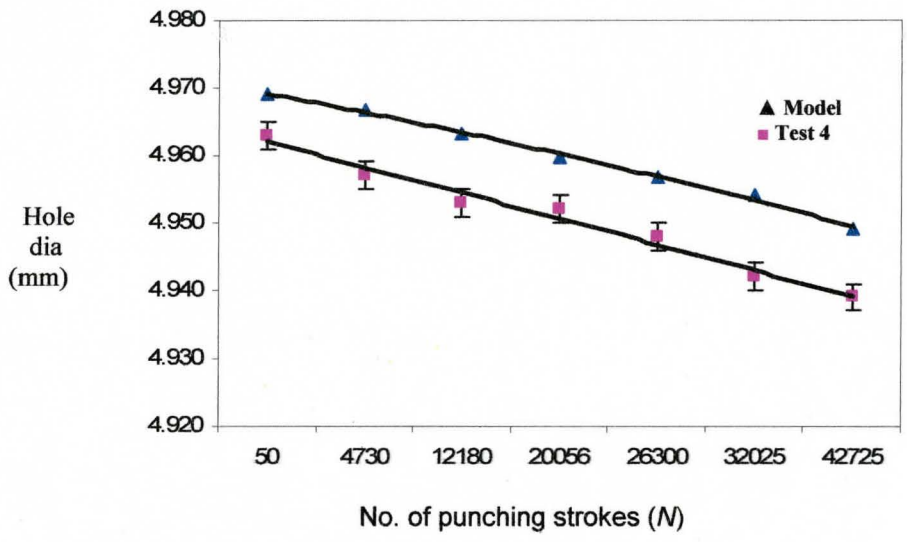

Figure 6-2 Hole size results – Comparison of models with Test 2 and 4

6.4 Tool Life Model Predictions

The major trends and observations from new tool life model are given below.

- Blanking force (F) is decreased with a higher clearance (Fig. 6-3 (a)).
- Tool life is increased with a higher clearance (ϖ). This is due to reduction in punch wear which is proportional to blanking force (Fig. 6-3 (b)).
- Tool life is decreased with an increase in material strength coefficient (K). This is because of increased blanking force which in turn causes the punch wear to increase (Fig. 6-3 (c)).
- Tool life is decreased with an increase in punch normalized wear rate (K') which in turn increase the punch wear (Fig. 6-3 (d)).

(a)

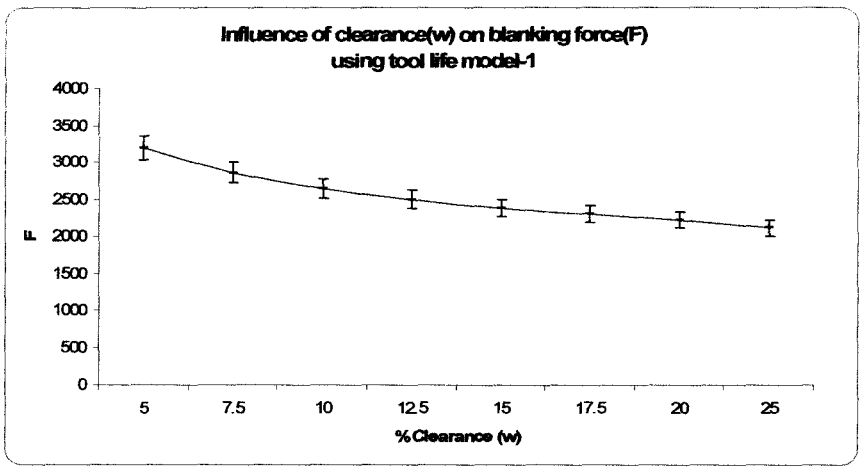

(b)

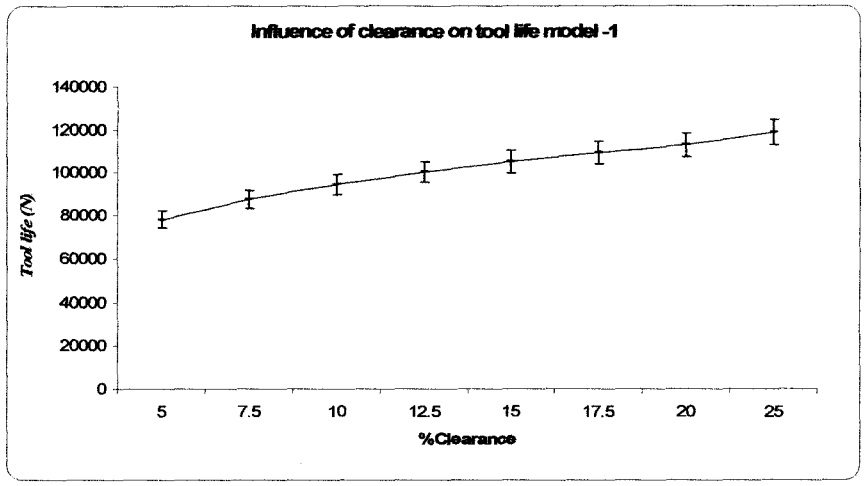

(c)

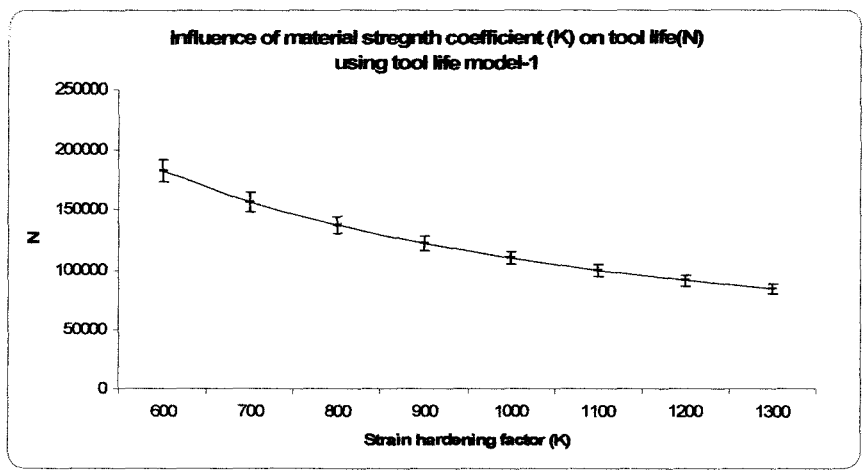

(d)

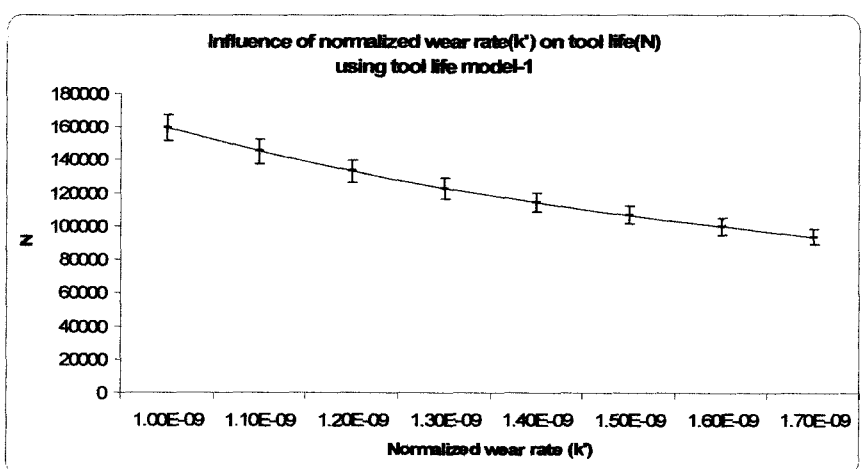

Figure 6-3 Trends from the tool life model.

6.5 Summary of Comparisons

The new analytical tool life model was compared in terms of burr height, hole size reduction and punch wear with the results from experiments. Also, the results from FE model were compared with the new analytical model in terms of burr height. The results are discussed in detail in Chapter 7. In addition to the comparison of results, the trends from the new analytical tool life model were also listed in terms of blanking force, clearance, material strength coefficient and punch normalized wear rates.

Chapter 7

Discussion

7.1 Piercing/Blanking Force (F)

Two blanking force models were considered in determining tool life as discussed in Chapter 3. The model predictions and experiment results are given in Table 7-1. The blanking force model proposed by Klingenberg and Singh I is used in the tool life model-1 whereas Ramaekers model is used in the tool life model-2.

Tool life model	Tool life equation	D_P	D_N	Tool life(N)
Model -1	$\frac{\pi}{4k'} \times \frac{\left(D_p{}^2 - D_N{}^2\right)}{\psi(d) L \tau (h_0 - d)}$	ϕ5.00	ϕ4.950	94,536
Model-2	$\frac{\pi}{4k'} \times \frac{\left(D_p{}^2 - D_N{}^2\right)}{L h_0 \sigma_{uts} S_f}$	ϕ5.00	ϕ4.950	35,783
Experiment	Test -1	ϕ5.00	ϕ4.954	100,000

Table 7-1 Comparison of blanking force models and experiment.

Table 7-1 clearly shows that predictions from model-1 are closer to the experiment than that of model-2. Hence, it is more appropriate to use Klingenberg and Singh's model to define blanking force which takes into account process parameters such as die clearance, friction and bending.

7.2 Pierced Hole Size

The new punch wear model predicting punch size reduction with reference to number of punching strokes is in good agreement with experiment as discussed in Chapter 6. However, the pierced hole size was measured less than the punch size as shown in Figure 7-1.

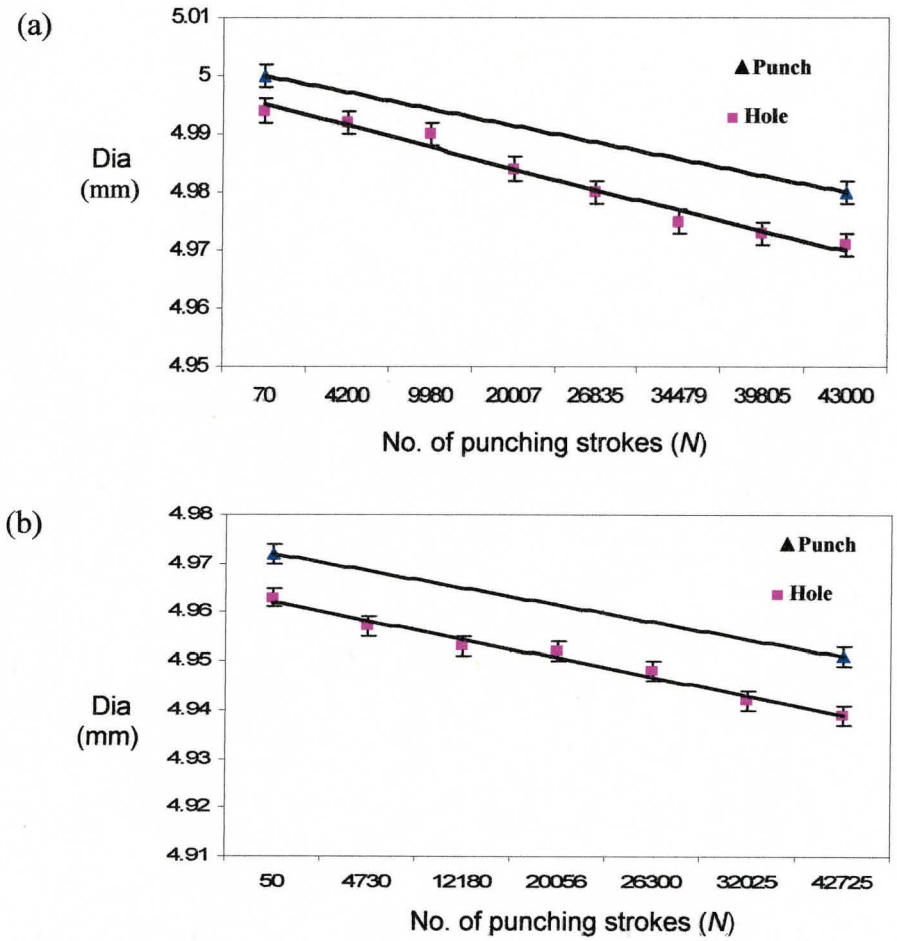

Figure 7-1 Comparison of punch and pierced hole size (a) Test 2 and (b) Test 4

7.2.1 Springback of Sheet after Punch Withdrawal

Elastic springback of the sheet material after punch withdrawal from the pierced hole is the main reason for hole diameter being measured less than the pierced punch. This was evident from the bending of sheet in the piercing process through FE simulations as discussed in Chapter 5 (see Fig 5-7). The amount of bending and springback was dependent on the clearance between punch and die. The difference between punch and hole size increased with an increase in clearance.

The amount of hole size variation due to springback of sheet may be included as a correction factor in the new tool life model (Fig 7-2). The correction factor may be dependent on the sheet thickness, sheet material properties, punch and die edge radius and the clearance. The latter can be decided by the accuracy and precision required by the user. The correction factor needs to be worked out according to the stamping environment and should be a subject of future study.

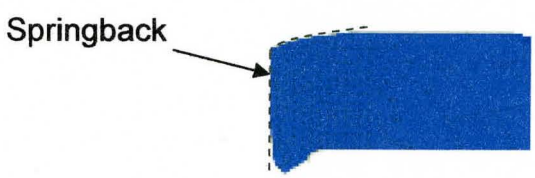

Figure 7-2 Change in hole profile due to springback.

7.3 Burr Width

In addition to the increase in burr height due to punch edge wear, it is observed that the burr width was also increased on slug as shown in Figure 7-3 and 7-4. In general, the increase in burr width is termed as 'hard' burr which is very difficult to remove by any deburring process. One reason for increased burr width could be the increase in punch edge radius due to wear. Hence, there is a need to quantitatively measure the burr width changes in addition to burr height.

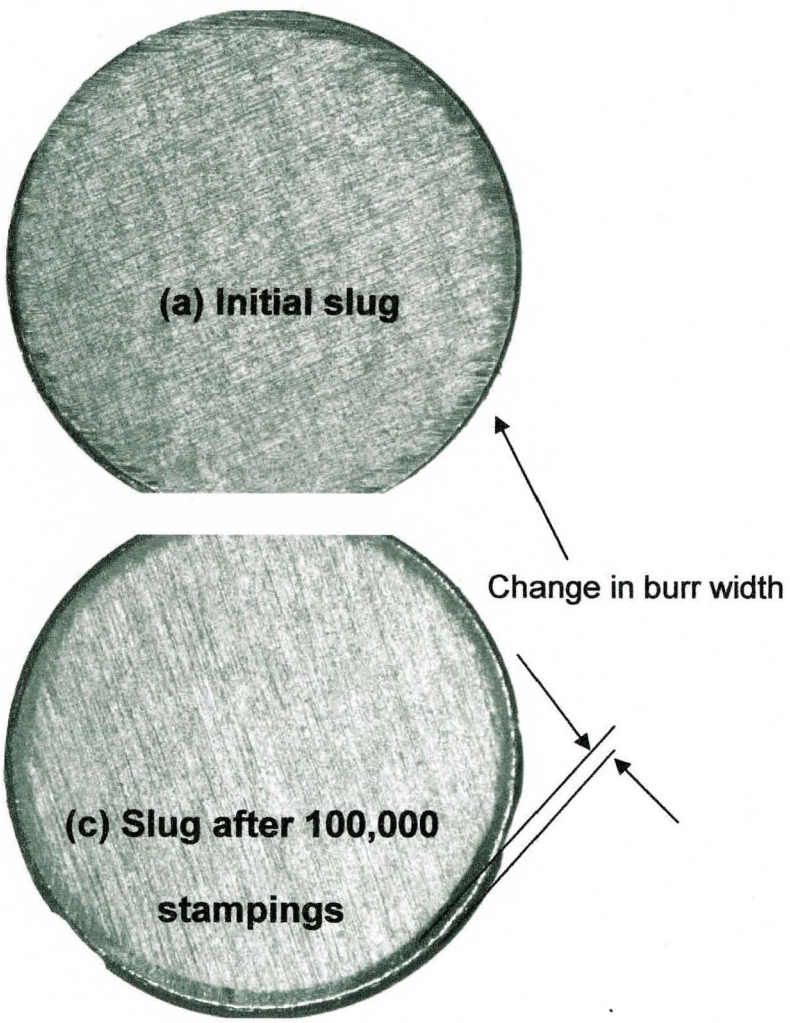

Figure 7-3 Change in burr width on slug/blank.

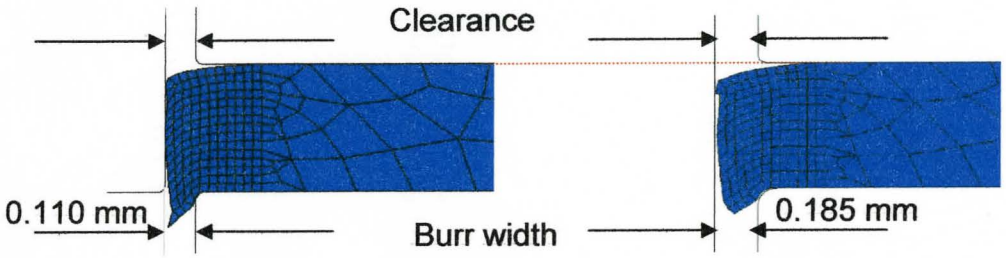

Clearance – 10%
Edge radius – 0.025 mm
(a)

Clearance – 17.5 %
Edge radius – 0.10 mm
(b)

Figure 7-4 Results from FE simulation - change in burr width with clearance.

7.4 Burr Height (b)

The experimental results have shown that burr height was influenced by clearance as well as punch edge wear. However, the tool life models in the literature have mostly utilized either the punch edge radius or the clearance. The new analytical tool life model proposed in the present study was defined by using the initial clearance as well as punch edge radius. Hence, the predictions from new tool life model are better compared to other tool life models.

7.5 Fatigue Failure

In the present study, the wear behavior under abrasion and adhesion conditions was considered and incorporated in the new tool life model. However, due to continuous punching, fatigue failure may be dominant after certain number of punch strokes which is not considered in the new model. A SEM image of punch edge with fatigue failure is shown in the Figure 7-5. The new analytical model can not be used to predict tool life where fatigue is a frequent cause of tool failures.

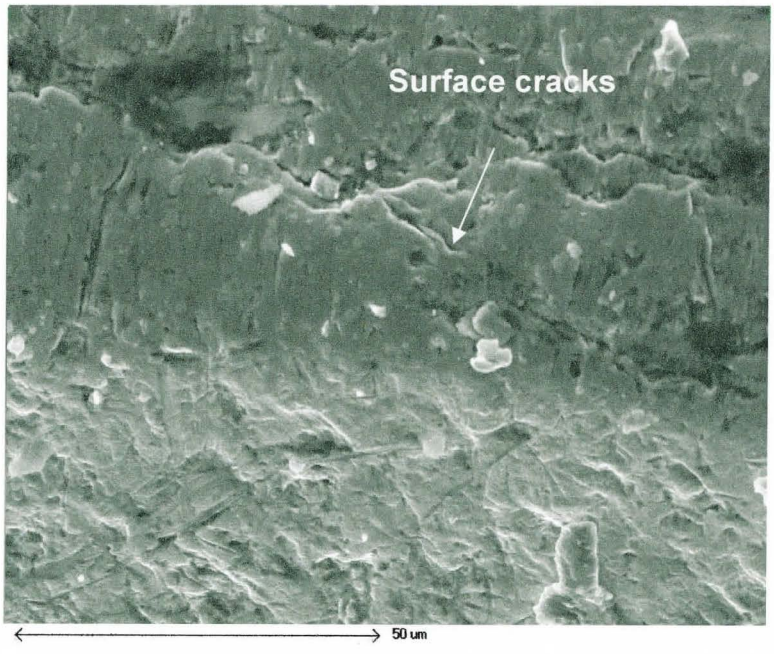

Figure 7-5 SEM image showing fatigue failure of punch edge (300X).

7.6 Application of Surface Coatings in Hole Piercing Process

Experiment with a MoS_2 coated punch was carried out to understand the effect of coatings on wear behavior in the hole piercing process. The selection of MoS_2 coating was done considering its latest application in stamping over other existing coatings. The coating layer of 5 micrometers remained adherent up to 10,000 punching strokes. It was observed that the coated surface was failed mainly due to crack and chip off (Figure 7-6).

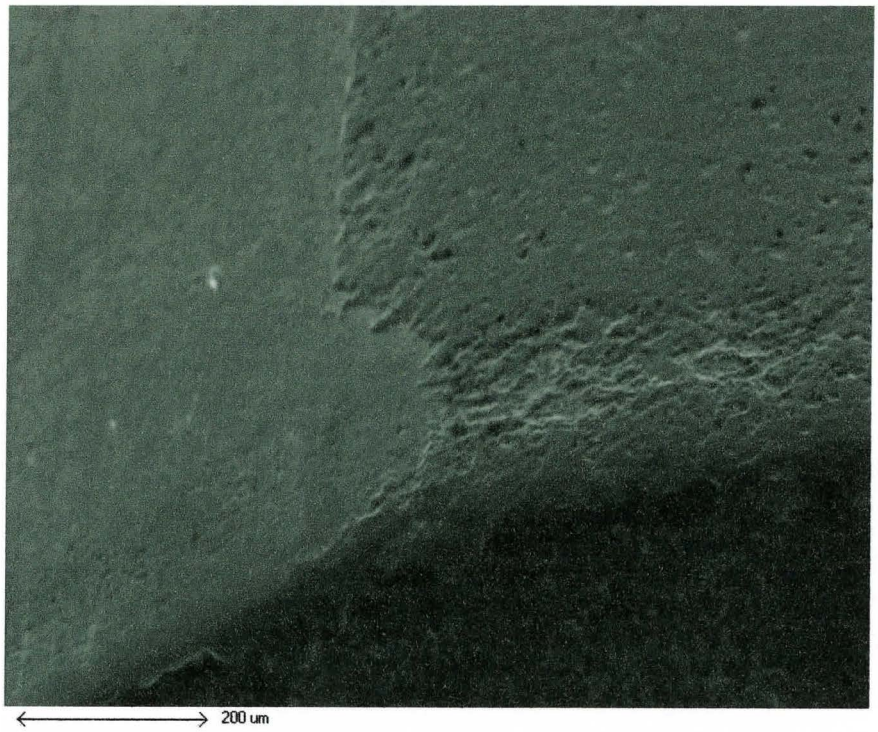

Figure 7-6 Chip-off of surface coating.

7.7 Wear on Bending Punches/Dies

In bending dies, the adhesive wear is dominant over abrasive wear [J. A. Schey, 1983]. The proposed new tool life model used to determine the wear on punch edge radius can be modified to suit process involving bending. Especially, the new model can be modified to determine tool wear in V – type bending dies (Figure 7-7). However, an additional research study is necessary to modify the new tool life model accordingly. For bending dies, earlier Equation (3-16) can be modified as:

$$V_b = sK''F_b \tag{7-1}$$

where V_b = Volume loss due to wear in bending punch/die

s = Total distance traveled by bending punch/die

K'' = Normalized adhesive wear rate in bending

F_b = Bending force

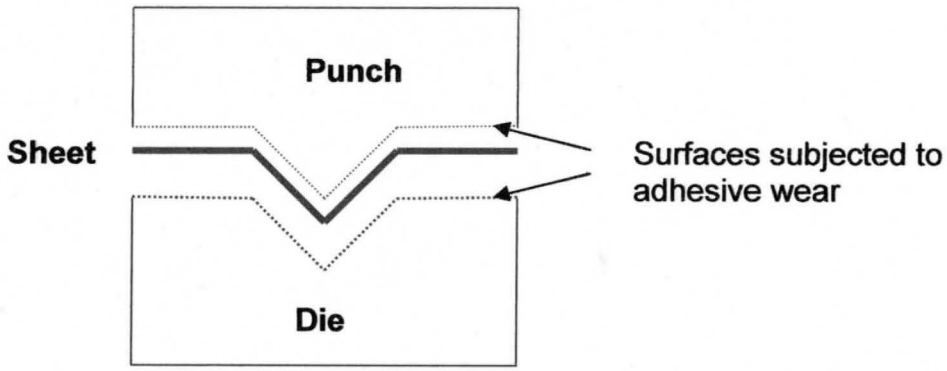

Figure 7-7 Wear on bending dies.

7.8 Differential Wear Rate on Punch

All of the tool life models discussed in literature review have used a single value of normalized wear rate. In general, the punch is subjected to adhesive wear near the edge and abrasive wear on the flank as discussed in Chapter 1. In the present study, a new analytical model has been defined using both wear processes using normalized wear rate in abrasion (K') and adhesion (K'').

7.9 Material Elongation Constant (C)

The piercing or blanking process is mostly defined by ductile fracture as indicated by several studies. The burr height is also dependent on ductility of the material apart from clearance and punch edge radius. Hence, the material elongation constant C was incorporated in the new tool life model. The value of material constant C was assumed as 0.9 in the present study and the experimental results were in good agreement with the value assumed. The tool life models discussed in the literature do not consider the material elongation factor.

Chapter 8
Conclusions and Future Work

8.1 Conclusions

- A new and improved analytical tool life models based on punch wear and burr height has been developed. Many of the factors that contribute to punch wear and burr height were studied. The proposed analytical tool life model to predict punch wear is a new way of defining tool life in stamping dies and different from the tool life models discussed in the literature review.

- The proposed tool life model combined with Klingenberg et.al [2004] blanking force model are in good agreement with experiments as discussed in Chapter 6.

- The tool life models predicts punch wear accurately and can be used to establish the need for tool regrinding by finding the pierced hole size variation.
- Burr height is in good agreement with new tool life model.
- FE modeling of piercing process was carried out. The results are in good agreement with the proposed analytical model and experiments.

8.2 Future Work

Several suggestions for future work are summarized below:

- Experiments should be carried out on different punch shapes, punch materials and sheet material to validate and improve the new analytical model.
- The burr width factor discussed in section 7-3 has to be studied further to incorporate into the new tool life model.
- The effect of increase in clearance due to punch wear should be studied further to improve the new tool life model
- The concept of differential normalized wear rate incorporated in the new tool life equation should be studied further.
- The punch speed should be considered to extend the usage of proposed tool life model to high speed stamping.
- The clearance starts increasing as the punch starts to wear in the production process. The effect of this increased clearance is not taken into account in the new tool life model. Further research is recommended on this subject.
- Applicability of new model to bending dies should be studied.

References

Bourithis, L., Papadimitriou, G.D., Sideris, J., *Comparison of wear properties of tool steels AISI D2 and O1 with the same hardness,* Tribology International (2005), pp 1-11.

Breitling, J., Pfeiffer, B., Altan, T., Siegert, K., *Process control in blanking,* Journal Materials Processing Technology, 71 (1997), pp 187-192.

Carrera, S., Salas, O., Moore, J.J., Woolverton, A.A., Sutter, E., *Performance of CrN/MoS2 (Ti) coatings for high wear low friction applications,* Surface Coatings & Technology, 167 (2003), pp 25-32.

Goijaerts, A.M., Govaert, L.E., Baaijens, F.P.T., *Evaluation of ductile fracture models for different metals in blanking.*, Journal of Materials processing technology, 110 (2001), pp 312-323.

Hambli, R., *Blanking tool wear modeling using the finite element method,* International journal of machine tools & manufacture, 41 (2001), pp 1815-1829.

Hambli, R., *Prediction of burr height formation in blanking processes using neural network,* International journal of mechanical sciences, 44 (2002), pp 2089-2102.

Hambli, R., Potiron, A., Abdessamad Kobi., *Application of design of experiment technique for metal blanking process optimization,* Mécanique &

Industries, 4 (2003), pp 175-180.

Hambli, R., *Blank soft: A computer software code for sheet metal blanking process optimization*, Journal of Materials Processing Technology, 141(2003), pp 234-242.

Hambli, R., *Prediction of optimum clearance in sheet metal blanking operation*; International Journal of Advanced manufacturing Technology, 22 (2003), pp 20-25.

Hatanaka, N., Yamaguchi, K., Takakura, N., Izuka, T., *Simulation of sheared edge formation process in blanking of sheet metals*, Journal of Materials & Processing Technology, 140 (2003), pp 628-634.

Hansen, P.H., Bay, N., *A flexible computer based system for prediction of wear distribution in forming tools*, Advanced Technology of Plasticity, 1990, Vol. 1, pp 19-26

Hogmark, S., Vingsbo, O., Fridstrom, O., *Mechanism of tool wear during cutting of austenitic stainless steel sheet*, Wear, 51 (1978), pp 85-104.

http://www2.thefabricator.com/

http://www.jardin-d-eden.co.uk/acatalog/Nomos_Watches.html

http://meiertool.com/ProgressiveDie.htm.

http://www.exactapunch.com.

http://www.ionbond.com.

Jordan, E.H., Urban, M.R., *An approximate analytical expression for elastic stresses in flat punch problems,* Wear, 236 (1999), pp 134-143.

Johnson, W., Slater; R.A.C., *Survey of slow and fast blanking of metals at ambient and high temperatures,* Proceedings of International Conference of Manufacturing Technology, CIRP-ASTME (1967), pp 825-851.

Ko, D-C., Kim, D-H., Kim, B-M., *Finite element analysis for the wear of Ti-N coated punch in the piercing process,* Wear, 252 (2002), pp 859 -869.

Ko, D-C., Kim, B-M., *Development of analytical scheme to predict the need for tool regrinding in shearing processes,* International journal of Machine Tools & Manufacture, 40 (2000), pp 1329-1349.

Klingenberg, W., Singh, U.P., *Comparison of two analytical models of blanking and proposal of a new model,* International Journal Machine Tools & Manufacture, 45 (2005), pp 519-527.

Luo, S.Y., *Studies on the wear conditions and the sheared edges in punching,* Wear, 208 (1997), pp 81-90.

Navas, C., Conde, A., Fernandez, B.J., Zubiri, F., Damborenea, J.D., *Laser coatings to improve wear resistance of mould steel,* Surface & Coatings Technology, 194 (2005), pp 136-142.

Rachik, M., Roelandt, J.M., Maillard, A., *Some phenomenological and computational aspects of sheet metal blanking simulation,* Journal of Materials Processing Technology, 128 (2002), pp 256-265.

Sarkar, A.D., *Book. Wear of Metals*, International Series on Materials Science and Technology, Vol.18.

Schey, J.A., *Book. Tribology in metal working, Friction, Lubrication and Wear*, American Society of Metals (1983).

Shyrokov, V., Maksymuk, A., Vasyliv, C., *Prediction of wear-resistant thin diffusive coatings*, Tribology International, 38 (2005), pp 179-185.

Situ, Q., *Masters Thesis., Study of trimming process in automotive aluminum alloys.*, McMaster University (2003),

Yan, W., Busso, E.P., Dowd, N.P.O., *A micro mechanic investigation of sliding wear in coated components*, The Royal society of London, (2000) 456, pp 2387-2407.

Appendix A

Material Data

A.1 Uniaxial Tensile Test:

Engineering strain was obtained by dividing the extension at each step by the original length 32 mm (Eq. A-1). Engineering stress was calculated by dividing the load by original area 6 mm x 1 mm (Eq. A-2). True strain and true stress were calculated using Equations (B-3) and (B-4).

$$\varepsilon^e = \Delta l / l \qquad \text{(A-1)}$$

$$\sigma^e = F / A \qquad \text{(A-2)}$$

$$\varepsilon^T = \ln(1+\varepsilon^e) \qquad \text{(A-3)}$$

$$\sigma^T = \sigma^e(1+\varepsilon^e) \qquad \text{(A-4)}$$

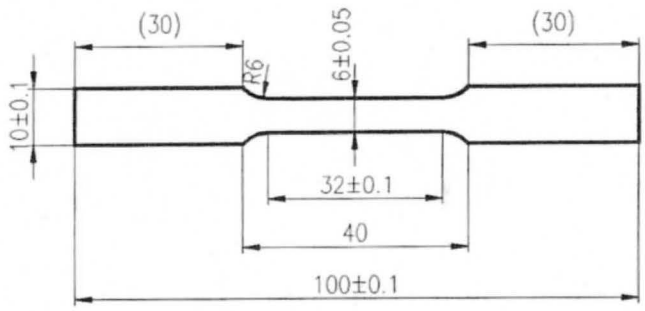

Figure A-1 Uniaxial tensile test sample as per ASTM E8M-04.

A.2 Calculation of Plastic Strain for FE Modeling

Plastic strain and true stress are required in ABAQUS/Explicit FE code for material property definition. Total True strain was further divided into elastic and plastic parts using Equation A-5, also shown in Figure A-2.

$$\varepsilon^{pl} = \varepsilon^{t} - \varepsilon^{el} = \varepsilon^{t} - \frac{\sigma}{E} \qquad \text{(A-5)}$$

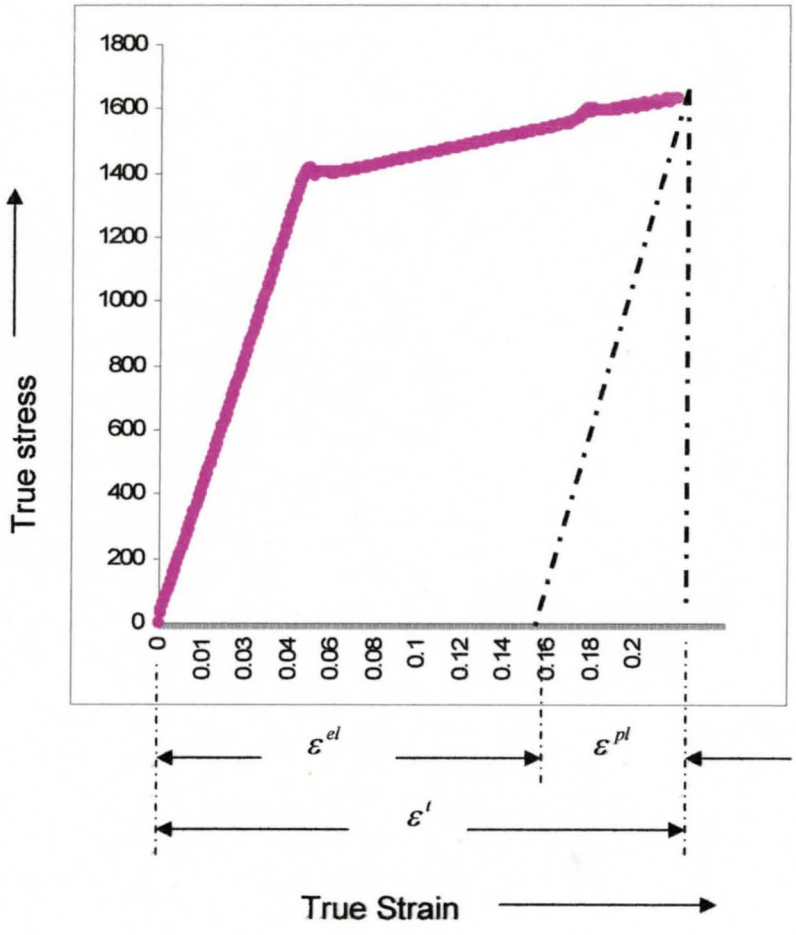

Figure A-2 Strain components.

A.3 Input file of Tool Set Configuration 1 (Table 5-2) for AISI 301 SS Material (Run in ABAQUS/Explicit 6.5)

```
*Heading
** Job name: nt-11 Model name: Model-1
*Preprint, echo=NO, model=NO, history=NO, contact=NO
**
** PARTS
**
*Part, name=Die
*End Part
**
*Part, name=Punch
*End Part
**
*Part, name=Sheet
*End Part
**
*Part, name=Stripper
*End Part
**
**
** ASSEMBLY
**
**
**
*Assembly, name=Assembly
**
*Instance, name=Die-1, part=Die
*Node
      1,          15.,          -5.,           0.
*Nset, nset=Die-1-RefPt_, internal
1,
*Surface, type=SEGMENTS, name=RigidSurface_, internal
START,       5.08,         -5.
 LINE,       5.08,       -0.42
 CIRCL,        5.1,       -0.4,         5.1,       -0.42
 LINE,         15.,       -0.4
*Rigid Body, ref node=Die-1-RefPt_, analytical surface=RigidSurface_
**
**
**
*End Instance
**
**
**
*Instance, name=Punch-1, part=Punch
*Node
      1,          2.,          5.,           0.
*Nset, nset=Punch-1-RefPt_, internal
1,
*Surface, type=SEGMENTS, name=RigidSurface_, internal
START,          5.,          5.
 LINE,          5., 0.02
 CIRCL,        4.98,          0.,        4.98, 0.02
 LINE,          0.,          0.
*Rigid Body, ref node=Punch-1-RefPt_, analytical surface=RigidSurface_
**
```

```
**
**
*End Instance
**
**
**
*Instance, name=Sheet-1, part=Sheet
*Node
     1,        5.25, -0.400000006
     2,        5.25,          0.
     3,   4.80000019,          0.

**
**
**

   462,   2.13171291,  -0.20047377
   463,   1.29797995, -0.205483243
   464,   4.73837233,  -0.25988695

*Element, type=CAX4R
 1,  1,  9, 135,  74
 2,  9, 10, 136, 135
 3, 10, 11, 137, 136

**
**
**

408, 439, 450, 458, 449
409, 462, 123, 124, 463
410, 453, 457, 454, 464
**
**
**
** Region: (Section-1:Picked)
*Elset, elset=_PickedSet2, internal, generate
  1, 410,   1
** Section: Section-1
*Solid Section, elset=_PickedSet2, material=SS301
1.,
**
**
**
*End Instance
**
**
**
*Instance, name=Stripper-1, part=Stripper
*Node
     1,         15.,          5.,          0.
*Nset, nset=Stripper-1-RefPt_, internal
1,
*Surface, type=SEGMENTS, name=RigidSurface_, internal
START,         15.,          0.
 LINE,         5.1,          0.
 CIRCL,        5.08,         0.02,         5.1,         0.02
 LINE,         5.08,         5.
*Rigid Body, ref node=Stripper-1-RefPt_, analytical surface=RigidSurface_
**
**
**
*End Instance
**
**
**
*Nset, nset=Sheet, internal, instance=Sheet-1, generate
  1, 464,   1
*Elset, elset=Sheet, internal, instance=Sheet-1, generate
  1, 410,   1
*Surface, type=NODE, name=Sheet_CNS_, internal
Sheet, 1.
**
**
**
**
```

```
*Nset, nset=_PickedSet12, internal, instance=Die-1
 1,
*Nset, nset=_PickedSet13, internal, instance=Punch-1
 1,
*Nset, nset=_PickedSet14, internal, instance=Stripper-1
 1,
*Nset, nset=RF-P, instance=Punch-1
 1,
*Nset, nset=RF-S, instance=Stripper-1
 1,
*Nset, nset=RF-D, instance=Die-1
 1,
**
**
**
*Nset, nset=_PickedSet18, internal, instance=Sheet-1
  7,  8, 125
*Elset, elset=_PickedSet18, internal, instance=Sheet-1
 385, 386
**
**
**
*End Assembly
**
** MATERIALS
**
**
**
*Material, name=SS301
*Density
 7.8e-06,
*Elastic
197000., 0.3
*Plastic
1450.3, 0.0
1470.4, 0.105
1500.3, 0.125
1600.5, 0.170
1623.4, 0.2
1635, 0.3
1635.75, 1.0
1636.5, 2.0
1638.75, 5.0
**
*Shear Failure, Element Deletion=yes
2.8
**
** INTERACTION PROPERTIES
**
*Surface Interaction, name=Friction
*Friction
 0.3,
** ----------------------------------------------------------------
**
** STEP: Piercing
**
*Step, name=Piercing
Piercing
*Dynamic, Explicit
, 0.4
*Bulk Viscosity
0.06, 1.2
**
** BOUNDARY CONDITIONS
**
** Name: Die Type: Displacement/Rotation
*Boundary
_PickedSet12, 1, 1
_PickedSet12, 2, 2
_PickedSet12, 6, 6
** Name: P-Down Type: Velocity/Angular velocity
*Boundary, type=VELOCITY
_PickedSet13, 1, 1
_PickedSet13, 2, 2, -1
_PickedSet13, 6, 6
** Name: Sheet Type: Displacement/Rotation
```

```
*Boundary
_PickedSet18, 1, 1
** Name: Stripper-1 Type: Displacement/Rotation
*Boundary
_PickedSet14, 1, 1
_PickedSet14, 2, 2
_PickedSet14, 6, 6
**
** INTERACTIONS
**
** Interaction: D-SH
*Contact Pair, interaction=Friction, mechanical constraint=KINEMATIC, cpset=D-SH
Die-1.RigidSurface_, Sheet_CNS_
** Interaction: P-Sh
*Contact Pair, interaction=Friction, mechanical constraint=KINEMATIC, cpset=P-Sh
Punch-1.RigidSurface_, Sheet_CNS_
** Interaction: S-SH
*Contact Pair, interaction=Friction, mechanical constraint=KINEMATIC, cpset=S-SH
Stripper-1.RigidSurface_, Sheet_CNS_
**
** OUTPUT REQUESTS
**
*Restart, write, number interval=1, time marks=NO
**
** FIELD OUTPUT: F-Output-1
**
*Output, field, number intervals=100
**
*Node Output
A, RF, U, V
*Element Output
LE, PE, PEEQ, S, STATUS
*Contact Output
CSTRESS,
**
** HISTORY OUTPUT: H-Output-1
**
*Output, history
*Node Output, nset=RF-P
RF2,
*Node Output, nset=RF-S
RF2,
*Node Output, nset=RF-D
RF2,
*End Step
```

Appendix B

Measurements Data using CNC Vision

B-1 Output file for Hole size (Table 4-13, Test -2)

Element	Actual	(TP Dev)
Circle: hole21(ID:11, From 7 Pts.)		
Diameter =	4.994	
Circular. =		0.040
Circle: hole22(ID:12, From 11 Pts.)		
Diameter =	4.992	
Circular. =		0.086
Circle: hole23(ID:13, From 10 Pts.)		
Diameter =	4.990	
Circular. =		0.024
Circle: hole24(ID:14, From 7 Pts.)		
Diameter =	4.984	
Circular. =		0.015
Circle: hole25(ID:15, From 7 Pts.)		
Diameter =	4.980	
Circular. =		0.018
Circle: hole26(ID:16, From 11 Pts.)		
Diameter =	4.975	
Circular. =		0.036
Circle: hole27(ID:17, From 10 Pts.)		
Diameter =	4.973	
Circular. =		0.046
Circle: hole28(ID:18, From 16 Pts.)		
Diameter =	4.971	
Circular. =		0.016

B-2 Output file for Burr Height

(For Burr sample 1 in Test 1)

(Shown in Table 4-11)

Element	Actual	Nominal	Deviat. (TP Dev)

Distance: (ID:21) between BURR411(ID:1) and BURR412(ID:2)

DZ = -0.051

Distance: (ID:22) between BURR411(ID:1) and BURR413(ID:3)

DZ = -0.057

Distance: (ID:23) between BURR411(ID:1) and BURR414(ID:4)

DZ = -0.067

Distance: (ID:24) between BURR411(ID:1) and BURRB416(ID:6)

DZ = 0.057

Distance: (ID:25) between BURR411(ID:1) and BURR417(ID:7)

DZ = -0.075

Distance: (ID:26) between BURR411(ID:1) and BURR418(ID:8)

DZ = -0.065

Distance: (ID:27) between BURR411(ID:1) and BURR419(ID:9)

DZ = -0.068

Distance: (ID:28) between BURR411(ID:1) and BURR421(ID:11)

DZ = -0.071

Distance: (ID:29) between BURR411(ID:1) and BURR422(ID:12)

DZ = -0.068

Distance: (ID:30) between BURR411(ID:1) and BURR423(ID:13)

DZ = -0.072